Optical Properties of Thermochromic Granular Films

Jørgen Vågan
Supervisor: Ingve Simonsen

September 24, 2015

Abstract

Abstract.. abstract.

1 INTRODUCTION

Today, in the light of global warming, the importance of reducing the amount of released greenhouse gases into the atmosphere is more crucial than ever. But because the use of fossil fuel is so well implemented in our society and constitute such an important energy source it is difficult to find replacements. However, identifying and improving the most energy unefficient components would help to reduce the overall energy consumption together with the related emissions of carbon dioxide. A relatively large portion of the energy consumption worldwide is due to the building sector. Today the energy consumption of buildings in developed contries constitute about 30-40% of their total energy usage. In humid regions, this increases to roughly 30%-50% [3, 4, 5]. In 2010, 41% of the primary energy of the U.S., being the second largest energy consumer globally and accounting for 7% of the global energy use, were consumed by the building sector. This resulted in approximately 40% of the total energy-related carbon dioxide emmision in the US. For comparison, the building sector in China accounted for 18% of the CO2 emmision of the country, whereas worldwide the building energy consumption is the cause of 8% of the total carbon dioxide emmision. [2, 6]. Because this in total makes such a significant impact worldwide, it should motivate to take measures in order to reduce the building energy consumption. In addition to lowering the energy consumption, it would also lower the energy related costs, for example related to the use of electricity. So reducing the overall building energy usage would have both economical and environmental benefits.

When considering the energy consumption of buildings, devices which are responsible for heating, ventilation and airconditioning (HVAC), and which in general help to maintain a comfortable indoor climate, are accounting for a significant amount of the overall energy usage. HVAC devices are used to compensate for heat loss through the building's envelope, e.g. walls, roof, windows or any element separating the indoor from the outdoor, or excessive heating due to the thermal radiation from the sun. Together with lighting, HVAC were responsible for about 60% of the total building energy consumption in 2010 **(???in the U.S. or in general???)**. [2]. The approaches to increase the energy efficiency of buildings can be divided into two categories: active strategies, including improving HVAC systems and lighting of the building; and passive strategies, such as improving the thermal properties of the building envelope. The latter includes measures like thermal insulation to walls, cool coatings on the roof tops or using windows with special coatings which alters the optical properties of the window [10, 11, 12, 13]. Commonly, windows fall into the category of some of the least energy efficient components of a building. Because of this, measures of improvement focusing on windows and improving their thermal properties seems the most reasonable [6]

The thermal properties of the window depend mainly on the outdoor conditions, such as shading, building orientation and type, in addition to the area of the window, its glass properties and glazing characteristics [8]. As the glazing characteristics determines the transmission of light through the window, they are, together with the air tightness of the window, the most relevant technical issues regarding energy losses. [9].One way of improving the thermal efficieny of the window is to add some additional mechanism, allowing the window to change its properties to the environment. Windows of this type are called "smart-" or "intelligent windows" and will be explained further in the following section [1].

REFERENCES

[1] Kamalisarvestani M, Saidur R, Mekhilef S, Javadi FS. *Performance, materials and coathing technologies of thermochromic thin films on smart windows*, PressOrSomething?, Renewable and Sustainable Energy Reviews ?? 2013; 26:353-364 ?? **ER DETTE RIGKTIG?**

[2] *DoE U. Buildings energy databook* Energy Effucuebct & Renewable Energy Department 2011. **MÅ SJEKKES!**

[3] Al-Rabghi OM, Hittle DC. *Energy simulation in buildings: overview and BLAST example*. Energy Conversion and Management 2001;42(13):1623-35 **MÅ SJEKKES!**

[4] Wilde PD, Voorden MVD.C. *Providing computational support for the selection of energy saving building components*. Energy and Buildings 2004;36(8):749-58

[5] Kwak SY, Yoo SH, Kwak SJ. *Valuing energy-saving measures in residential buildings: a choice experiment study*. Energy Policy 2010; 38(1):673-7

[6] Hong T. *A close look at the China design standard for energy efficiency of public buildings*. Energy and Buildings 2009;41(4):426-35

[7] Baetens R, Jelle BP, Gustavsen A. *Properties, requirements and possibilities of smart windows for dynamic daylight and solar energy control in buldings: a state-of-the-art review*. Solar energy Materials and Solar Cells 2010;94(2):87-105

[8] Hassouneh K, Alshboul A, Al-Salaymeh A. Influence of windows on the energy balance of apartment buildings in Amman. Energy Conversion and Management 2010;51(8):1583-91.

[9] . Tarantini M, Loprieno AD, Porta PL. A life cycle approach to Green Public Procurement of building materials and elements: a case study on windows. Energy 2011;36(5):2473-82.

[10] Bojic M, Yik F, Sat P. Influence of thermal insulation position in building envelope on the space cooling of high-rise residential buildings in Hong Kong. Energy and Buildings 2001;33(6):569-81

[11] Cheung CK, Fuller R, Luther M. Energy-efficient envelope design for high rise apartments. Energy and Buildings 2005;37(1):37-48

[12] Synnefa A, Santamouris M, Akbari H. Estimating the effect of using cool coating on energy loads and thermal comfort in residential buildings in various climatic conditions. Energy and Buildings 2007;39(11):1167-74

[13] Sadineni SB, Madela S, Boehm RF. Passive building energy savings: a review of building envelope components. Renewable and Sustainable Energy Reviews 2011;15(8):3617-31

2 SMART WINDOWS AND THERMOCHROMISM

2.1 SMART/INTELLIGENT WINDOWS

A smart window or intelligent window is a type of window that manages to regulate the transmitted solar radiation by changing its optical properties. The change in the optical properties can be obtained by adding a controllable absorbing layer on the surface of the glass. The resulting ability of the smart window to control the transmittance ofsolar flux and daylight, may help to reduce the electricity consumption regarding heating, cooling and lighting. They should optimally also be able to adapt to the differences created by the seasons. E.g. summertimes have a different demand than wintertimes with respect to the thermal properties of the window. In summertimes the ambient temperature is around or above the comfortable region and the window should therefore possess high reflectance in the infrared region to prevent further increase in temperature. In wintertimes on the other hand, the temperature is below the comfortable level and the reflectance should be low in order to allow the sun to heat up the indoor climate. This in addition to the transmission of light in the visible region, may reduce or remove the need for electrical heating, cooling or lighting such as HVAC devices or light bulbs. [4, 5, 8]
Windows with such a switchable layer can be categorized into two systems: active and passive. The active systems may be for example a switchable glazing with the opportunity to switch from one set of optical properties to another. An example of this is a electrochromic window, which uses a burst of electricity from an external energy source in order to change the opacity of the material. The passive devices on the other hand, do not require an external energy source, but switches automatically subject to environmental change. Examples of such devices are: photochromic windows, which reacts to light and thermochromic windows, which change in accordance to the temperature [1, 6]. The latter materal will be discussed in more detail in the following section. As shown

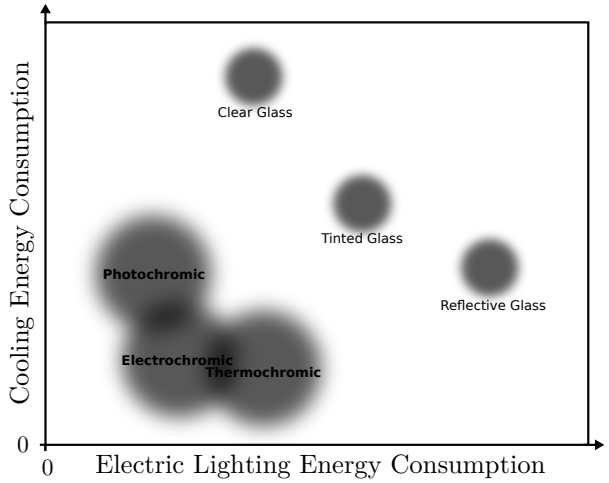

Figure 2.1: Comparison of the electric lighting energy and cooling energy consumption between different glazing types. Adapted from [3, p. 20]. For example, reflective glass reflects a large portion of the incident radiation, both visual light and radiant heat. This leaves it as a good option for hot climates where it can reduce the cooling load of the building. However, due to the low transmission of light additional lighting is required lowering the energy benefit to some extent.

in Figure 2.1 the resulting energy consumption varies for the different window and glazing technologies. It also demonstrates an important fact: even though using reflective glass would reduce cooling loads, a window should also be able to let visible light through. If the transmission of the visible spectrum is to low, it could cause the need for additional lighting, which again would increase the overall energy load [15]. Electrochromic and thermochromic windows usually result in lower cooling loads. In addition the electrochromic technology requires less energy for lighting due to the thermochromic coatings low optical transmission. However, this is not enough to exclude thermochromic layers as they serve as a good and low-priced alternative to the electrochromical ones [14]. For instance, a thermochromic window does not need any elecrical wires as its electrochromic counterpart and the low visible transmission of the thermochromic windows can be increased by adding small quantities of a foreign material into the thermochromic coating. The process of adding small quantities of another element into

a material is called doping and leads to changes in the electrical and optical properties [13, p. 39].

2.2 THERMOCHROMIC MATERIALS

The technology behind intelligent windows and its diversity, is based on materials that change their optical properties when subjected to some external physical process. These materials are called chromic materials. The word chromic originates from the greek word "Chroma", which means color. If the induced change of optical properties results in changing the spectral reflectance in the visible spectrum, the material will change its color. Chromic materials are again subdivided into categories dependent on what triggers their optical change. For example, photochromic and eletrochromic materials are two categories of chromic materials that changes their optical properties when subject to irradiation by light (photons) or an applied electric field, respectively. However, another subcategory is thermochromic materials and will be the category of interest in this assignment [16].

"Thermos" is the greek word for warm or hot. As the name suggests, thermochromic materials change their optical properties, such as color, in response to heat or, in other words, the change in temperature. [7] [8]. Typically, this change in color happens gradually over a range of temperatures. In this case it is called continuous thermochromism. Discontinuous thermochromism also occurs and involves a structural phase change at a certain characteristic "transition temperature" T_t. This phase change can be of first or second-order in nature, and may be reversible or irreversible [16]

Compounds like inorganic oxides, liquid cryctals [17]conjugated oligomers, leuco dyes [18] can exhibit thermochromic color changes reversibly, while thermochromic dyes, usually based on organic compounds, show color temperature dependent changes which are not reversible [2].

To explain the process behind the chromic behaviour, assume that the thermochromic material is initially in its cold state called the monoclinic state . Here it behaves as a semiconductor, being less reflective especially in the near-infrared(IR) region. Heating the material to a certain temperature, known as the transition temperature, will make it change from the monoclinic state to a rutile state. In the rutile or hot state the material acts like a semi-metal, reflecting a wide range of solar radiation. This change of state is called metal-to-semiconductor transition (MST) [10, p. 4565] and is fully reversible and co-occures with large variations in both electrical and optical properties in the near-IR range [11].
Because of these interesting properties, thermochromic materials have become increasingly important, espacially through the use as "smart coatings". Some potential thin film candidates for smart windows include substances such as Fe_3O_4, $FeSi_4$, NbO_2, NiS, TiO_2 and VO_2. [8].

2.3 THERMOCHROMIC WINDOWS

A thermochromic window, is a window with a thermochromic glazing, allowing the window as a whole to adopt the optical properties of the thermochromic material. Figure 2.2 is a pictorial representation of the influence of the thermochromic coating on the window. Below the transition temperature $T < T_t$, the window should trans-

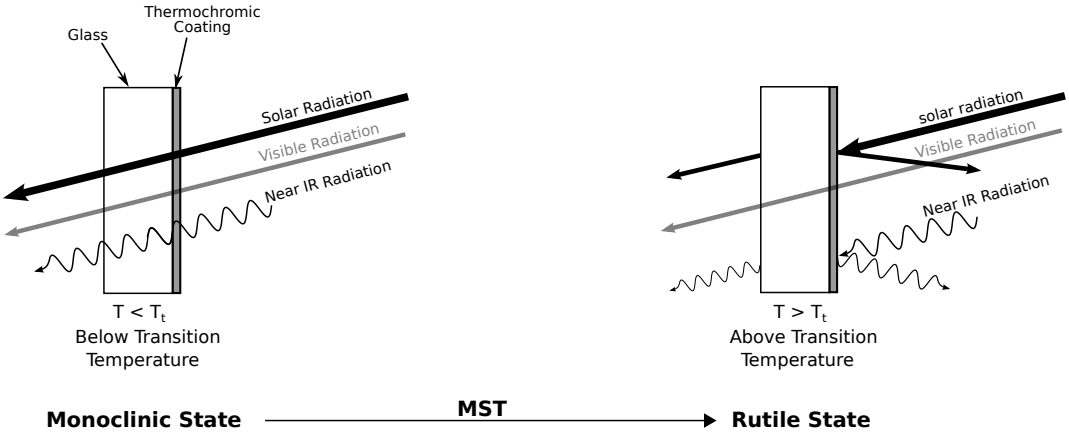

Figure 2.2: Schematic representation of thermochromic materials applied as an intelligent window coating [2].

mit the solar thermal radiation, heating up the interior of the building. If the temperature increases above the transition temperature T_t, the transmission of the thermal radiation should decrease significantly, lowering or removing the necessity of using cooling devices. For this to work, the transition temperature, which for most materials is significantly higher than room temperature, needs to be reduced down to a thermally comfortable level. Similarly to the transmission of the coating, this may be solved through doping with a foreign material or dopant. An example of such a dopant will be discussed in Section 2.4.1, which contains a closer look at a promosing thermochromic coating candidate called vanadium dioxide.

The ideal spectral modulation of the thermochromic coating is given in Figure 2.3. This shows how the cold state should transmit the majority of the solar radiation, here modeled as a black body spectrum. In addition it shows how the hot state should reflect as much of the infrared and solar radiation as possible without compromising the transmission of the visible spectrum. If the transmission of daylight is poor, it would lead to an increase of the electrical load due to the accompanying additional lighting. [1]

As discussed by Blackman [10, p. 4569], the optical transmission of the film is depending on the thickness of the film. Control of the film thickness is crucial. Excessive coating thicknesses may lead to too much blocking of the visual light, leaving the coating unsuitable for architectural application. For the transmission of visible light to

Table 2.1: The ideal optical performance of thermochromic windows (taken from [1]) which adapted it from [12]

State	**Monoclinic/cold** ($T < T_t$)		**Rutile/hot** ($T > T_t$)	
Wavelength	Visible(%)	NIR (%)	Visible(%)	NIR (%)
Transmittance(T)	60-65	80	60-65	15
Reflectance(R)	17	12	17	77

be acceptable it should be higher than 60%. The ideal performance of a thermochromic window is shown in Table 2.1, showing that the modulation of the spectrum in the visible region should be the same for both the monoclinic and rutile state. Notice the transmission of 60%-65% of the visible light.

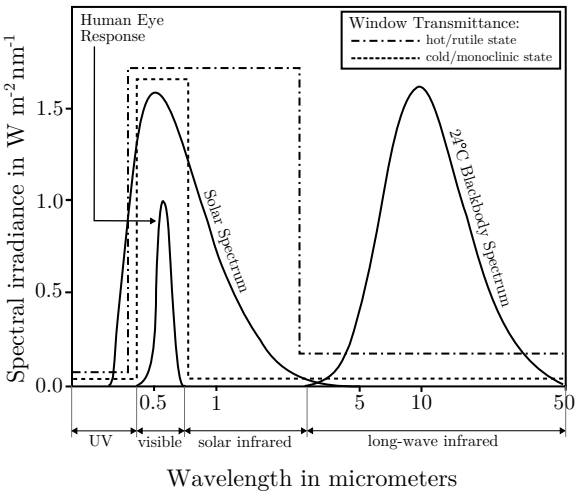

Figure 2.3: The spectral transmittance of a perfect thermochromic window, shown for both cold and hot environments (the monoclinic and rutile state, repsectively). Adopted from [1, p. 15]

REFERENCES

[1] McCluney R, Center FSE. Fenestration solar gain analysis. Citeseer 1996.

[2] Kiri P, Hyett G, Binions R. Solid state thermochromic materials. Advances Material Letters 2010;1(2):20.

[3] Huovila P, Ala-Juusela M, Melchert L, Pouffary S. Buildings and climate change: status, challanges and opportunities. United Nations Environment Programme 2007.

[4] Dussault J-M, Gosselin L, Galstian T. Integration of smart windows into building design for reduction of yearly overall energy consumption and peak loads. Solar energy 2012;86(11):3405-16

[5] Jelle BP, Gustavsen A. Dynamic solar radiation control in buildings by applying electrochromic materials. Renewable Energy Conferance/Advanced materials technologies 2010; :133**er dette riktig?**

[6] Baetens R, Jelle BP, Gustavsen A. Properties, requirements and possibilities of smart windows for dynamic daylight and solar energy control in buildings: a state-of-the-art review. Solar energy materialsand solar cells 2010;94(2):87-105.

[7] Parkin IP, Manning TD. Intelligent thermochromic windows. Journal of Chemical Education 2006;83(3):393.

[8] White MA, LeBlanc M. Thermochromism in commercial products. Journal of Chemical Education 1999;76(9):1201,1204

[9] Lampert CM. Smart windows switch on the light. IEEE Circuits Devices Mag. 1992; 8(2):19

[10] Blackman CS, et al. Atmospheric pressure chemical vapour deposition of thermochromic tungsten doped vanadium dioxide thin films for use in architectural glazing. Thin Solid Films 2009;517(16):4565-70.

[11] Morin F. Oxides which show a metal-to-insulator transition at the Neel temperature. Physical Review Letters 1959;3(1):34-6

[12] Saeli M, et al. Energy modelling studies of thermochromic glazing. Energy and buildings 2010;42(10):1666-73.

[13] Kanu SS, Binions R. Thin films for solar control applications. Proceedings of the Royal Society of London series A 2010;466(2113):19-44

[14] Mlyuka N, Niklasson G, Granqvist CG. Thermochromic multilayer films of VO_2 and TiO_2 with enhanced transmittance. Solar Energy Materials and Solar Cells 2009;93(9):1658-7

[15] Correa G, Almanza R. Copper based thin films to improve glazing for energy-savings in buildings. Solar Energy 2004;76(1-3):111-5

[16] Mott N.F. Metal-insulator transitions. 1974.

[17] Seredyuk M, Gaspar AB, Ksenofontov V, Reiman S, Galyametdinov Y, Haase W, Rentschler E, Gütlich P. Room temperature opperational thermochromic liquid crystals. 2006;18(10),2513

[18] Seeboth A, Klukowska A, Ruhmann R, Lötzsch D. Thermochromic polymer materials. Chinese journal of polymer science (english edition). 2007;25(2),123-135

2.4 VANADIUM DIOXIDE VO_2; A PROMISING CANDIDATE

The most promising thermochromic material regarding thermochromic intelligent windows is vanadium (IV) oxide. Vanadium oxide can exist in four polymorphic forms; monoclinic, rutile and two metastable forms [1]. The metal to semiconductor phase transition from the monoclinic to the rutile state occurs at 68°C and is fully reversble. In this transition, large changes in electrical conductivity and optical properties in the near-IR region occur [11], **while the change in optical region is relatively small [7, p. 395]**. Above T_t it behaves as a semi-metal, reflecting to a wide range of solar wavelengths , while below, it behaves as a semiconductor, reflecting significantly less in the near infrared region [10, p. 4565].

The transition temperature of 68°C is relatively low compared other thermochromic materials. 68°C is, however, far from the comfortable temperature region around ~ 20°C. This would leave the window in its monoclinic state for all natural ambient temperatures, never switching it's state and leaving it unsuited as a smart coating [1, p. 358] [13, p. 39].

Many studies regarding vanadium dioxide coatings have reported low transmittance in the visible range as discussed in the review of Kamalisarvestani et al. [1, p.358] and may be the largest weakness of VO_2 coatings. The switching efficiency η_T, defined as the change in transmittance over the transition temperature T_t, is a measure of the energy-saving efficieny and depends the film thickness [10, p. 4569]. However, because increasing the film thickness also reduce the transmittance of visual light, this parameter must be carefully tuned. For VO_2, the ideal film thickness regarding visual transmission and switching efficieny is between 40-90nm. Here the maximal thickness should be set correspondingly to the minimum acceptable optical transmission [1, p. 358] [10, p. 4569].

2.4.1 TUNGSTEN DOPING OF VO_2 COATINGS

The most efficient dopant of VO_2 coatings is the chemical element tungsten W. Tungsten is also known as wolfram and can be found in the periodic table under atomic number 74. When used as a dopant in VO_2 it reduces the transition temperature T_t of the MST and can optimally lower T_t down to about 25°C at 2 atom % loading [10, p. 4566]. There are also other problems regarding VO_2 coatings affecting their applicability other than T_t: vanadium dioxide have an unappealing yellow or brown color. However, this is also improved using tungsten as a dopant and give the coating a greener/bluer color. This is depending on the relative amount of tungsten and allows some control of the aesthetical properties [10, p. 4565,4569].

REFERENCES

[1] Leroux C.h, Nihoul G, Van Tendeloo G. From VO2(B) to VO2(R): Theoretical structures of VO2 polymorphs and in situ electron microscopy. Physical Review B 1998;57(9),5111

3 INTRODUCTIONAL THEORY

In order to get a better understanding of the optical response of a material with a dielectric constant $\varepsilon(\omega)$, this section will briefly discuss the Drude model, the polarization contributions to the dielectric function and, last, the relation between the $\varepsilon(\omega)$ and the refractive index $N(\omega)$.

3.1 THE DRUDE MODEL

P. Drude, in his attempt to explain the properties of metal, created a simple model where he assumed that the electrons in a solid behave like a classical gas. In his model, the electron-electron and Coloumb interactions are neclected. The only form of interaction in this model is the instantaneous collision between the electrons and the positively charged ion cores which are assumed to be static; see Figure 3.1. The electrons reach thermal

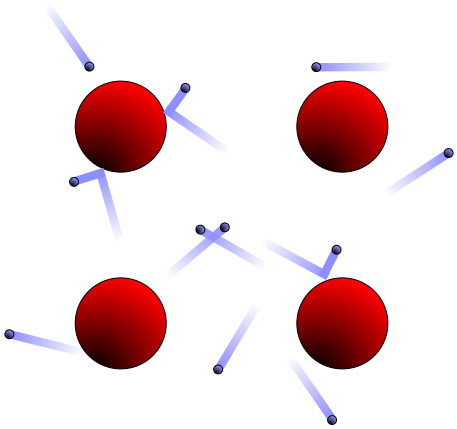

Figure 3.1: The Drude model: A non-interacting electron gas (blue) is swirling around and colliding with stationary positive ion cores (red). Since all Coloumb forces are neglected together with electron-electron collsions, the ion-electron interaction is the only one being considered.

equilibrium with the lattice through the collisions, giving them the kinetic energy:

$$\frac{1}{2}m_e v_t = \frac{3}{2}k_B T. \tag{3.1}$$

The average time between two collisions is called the relaxation time τ, with the corresponding mean free path defined as $\lambda = \tau v_t$. The probability for a electron to collide per unit time is assumed to be $1/\tau$ [1, p. 71-72].

3.1.1 OPTICAL REFLECTIVITY OF DRUDE METALS

The optical properties of materials are described by the complex refractive index $N(\omega)$ or the dielectric constant $\varepsilon(\omega)$. To explain the reflectivity of metals we can concider an electron in an electromagnetic field induced by an optical incident wave with wavenumber $q = 2\pi N/\lambda_0$, where λ_0 is the wavelength of the wave in free space.
If ω is low, we basically retain the DC behavior governed by Ohm's law. However, if ω is so high that $1/\omega \ll \tau$, the electrons does not manage to react fast enough and the collisions with the ions altogether can be ignored. This is fulfilled for optical frequencies when $\tau = 10^{-14}$s). The electrons can now be treated as completely free, and a single electron follows

$$m_e \frac{d^2x(t)}{dt^2} = -eE(t) = -eEe^{-i\omega t}. \tag{3.2}$$

A good ansatz for the solution is setting $x(t) = Ae^{-i\omega t}$, which mean that the electron is oscillating along with the electric field. This gives an amplitude of

$$A = \frac{eR}{m_e\omega^2}. \tag{3.3}$$

The corresponding polarization due to the dipole moment of $-eA$ for a solid with conduction electron density n_e is

$$P = -n_e eA = -\frac{n_e e^2 E}{m_e \omega^2}. \tag{3.4}$$

From the constitutive relation

$$D = \varepsilon\varepsilon_0 E = \varepsilon_0 E + P, \tag{3.5}$$

we get that

$$\varepsilon = 1 + \frac{P}{\varepsilon_0 E} = 1 - \frac{n_e e^2}{\varepsilon m_e \omega^2} \equiv 1 - \frac{\omega_p^2}{\omega^2}, \tag{3.6}$$

with the plasma frequency ω_p defined as

$$\omega_p = \frac{n_e e^2}{m_e \varepsilon_0}. \tag{3.7}$$

We can distinguish between two different cases and the resulting outcome can be seen from the the electromagnetic plane wave

$$\boldsymbol{E}(z,t) = \boldsymbol{E}_0 e^{i(2\pi N z/\lambda_0 - \omega t)}. \tag{3.8}$$

In the first case, $\omega < \omega_p$ and ε is a real and negative, $\varepsilon = \varepsilon_{\Re e} < 0$. Therefore, $N = \sqrt{\varepsilon}$ is purely imaginary, and the wave penetrating the solid is exponentially damped. Because Eq.(3.2) contain no inelastic properties, nothing is absorbed. The light that is not transmitted into the medium must therefore, due to energy conservation, be reflected back.
For the second case, $\omega > \omega_p$, the dielectric constant is real and positive, meaning that $\varepsilon = \varepsilon_{\Re e} > 0$. Followingly, the index of refraction is real and positive, i.e. $N = n > 0$. The result is a plane wave that propagates into the metal. This explains why metals are so reflective, or shiny. They are reflective for low-frequency light, but transparent for high-frequency light. The transition happens at the plasma frequeny, which can be calculated solely from the conduction electron density of the metal. For most metals, the plasma frequency is in the far UV region, making them reflective in the visible range. Frequently, the plasma energy $\hbar\omega_p$ is used instead of the plasma frequency ω_p [1, p. 76-79].

3.1.2 Shortcomings of the Drude model

The quenstionable assumptions of the Drude model is the removal of the electron-electron interaction together with all the Coloumb forces. In addition, the assumption of treating the electrons as particles is not justified due to the fact that their de Broglie wavelength, in the case of thermal electrons, is in the order of nanometers. The assumption would however only satisfy electrons moving in structures much larger than the de Broglie wavelength.

The resulting conductivity of the model is not high enough at low temperatures, and is due to the assumption of a fixed mean free path, given by the atomic spacing. Apparantly, at low temperature, the electrons manage to sneak past the other electrons and ions.

Also, the conductivity of alloys, in which impurities drastically reduce the conductivity, finds no justification in the Drude model [1, p. 80-81].

3.2 Complex permittivity and index of refraction

The complex dielectric constant or relative permittivity $\varepsilon(\omega) = \varepsilon_{\Re e}(\omega) + i\varepsilon_{\Im m}(\omega)$ of a material, is a measure of the material's response subject to an electromagnetic field. Here ε_r and $\tilde{\varepsilon}_r$ denotes the real and imaginary components, respectively. The relative permittivity is related to the square of the refractive index $N(\omega) = n(\omega) + ik(\omega)$

$$\varepsilon(\omega) = N(\omega)^2 \tag{3.9}$$

which determines the optical properties of a given material. The real and imaginary refractive indicies are denotes by n and k, respectively The choice of sign convention, i.e. using $n+ik$ rather than $n-ik$, is determiend by the choice of the sign in the in the plane wave solution, $\exp i(\boldsymbol{q}\cdot\boldsymbol{r}-\omega t)$, of Maxwell's equations, where q is the wave vector. Expanding Eq.(3.9) one gets

$$\varepsilon_{\Re e} + i\varepsilon_{\Im m} = n^2 - k^2 + i2nk, \tag{3.10}$$

which through simple comparison, gives

$$\varepsilon_{\Re e} = n^2 - k^2 \qquad\qquad \varepsilon_{\Im m} = 2nk. \tag{3.11}$$

Taking the absolute value or modulus

$$|\varepsilon| = \sqrt{(\varepsilon_{\Re e})^2 + (\varepsilon_{\Im m})^2} = \sqrt{(n^2-k^2)^2 + (2nk)^2} = n^2 + k^2, \tag{3.12}$$

and putting it all together, gives the real and imaginary parts of N expressed through the relative permettivity

$$n = \left(\frac{|\varepsilon| + \varepsilon_{\Re e}}{2}\right)^{\frac{1}{2}} \qquad\qquad k = \left(\frac{|\varepsilon| - \varepsilon_{\Re e}}{2}\right)^{\frac{1}{2}} \tag{3.13}$$

Considering a plane wave with a complex wave vector $q = q_{\Re e} + iq_{\Im m}$ moving in the material [2, p. 402]

$$e^{i(qz-\omega t)} = \exp\{-q_{\Im m} z\} \cdot \exp\{i(q_{\Re e} z - \omega t)\}, \tag{3.14}$$

one sees that the wave is attenuated. The quantity $\alpha \equiv 2q_{\Im m}$ is called the absorption coeffiecient and is proportional to the optical conductivity σ, to $q_{\Im m}$, and to k:

$$n\alpha = \frac{4\pi\sigma}{c} = \frac{\omega}{c}\varepsilon_{\Im m} \tag{3.15}$$

$$\Downarrow \tag{3.16}$$

$$\frac{\alpha}{2} = \frac{\omega}{c}k = \frac{1}{\delta} \tag{3.17}$$

k is usually called the extinction coefficient and is essentially the ratio of the free-space wave frequency ω to the skin depth δ.
Just to mention it, n and k can be found experimentally by measuring the reflectivity R of a bulk, opaque sample, in addition to the transmittance T of a slab, which are given in terms of n and k as

$$R = \frac{(n-1)^2 + k^2}{(n+1)^2 + k^2} \tag{3.18}$$

$$T = \frac{(1-R)^2 e^{-2\omega kd/c}}{1 - R^2 e^{-4\omega kd/c}}, \tag{3.19}$$

where d is the sample thickness. The slab multiple-reflection effects are averaged, so that interface fringes are not resolved [2, p. 169-170].

3.3 Microscopic polarization and the dielectric function

There are several mechanismc causing microscopic electric dipole moments that lead to macroscopic polarization. E.g. displacement of the electronic cloud to the core in an atom, opposite displacement of the ions in a solid or orientation of permanent dipoles, such as water molecules, called orientational polarization.

3.3.1 The local field

To calculate the microscopic polarizability α of the atoms making up the solid, start with the constitutive relation and assume that $\boldsymbol{P}$ can be written as the total dipole moment per unit volume

$$\boldsymbol{P} = (\varepsilon - 1)\varepsilon_0 \boldsymbol{E} = \frac{N}{V}\boldsymbol{p} = \frac{N}{V}\alpha\boldsymbol{E}. \tag{3.20}$$

Because a microscopic dipole within the solid does not simply feel the average electric field $\boldsymbol{E}$ but a microscopic local and stronger electric field $\boldsymbol{E}_{loc}$, the polarizability can bot be correctly calculated from the above expression. Without derivation, the approximate local field can be given by

$$\boldsymbol{E}_{loc} = \frac{1}{3}(\varepsilon + 2)\boldsymbol{E}. \tag{3.21}$$

So, with

$$\boldsymbol{P} = \frac{N}{V}\alpha \boldsymbol{E}_{loc} \tag{3.22}$$

and approximating the polarization $\boldsymbol{P}$ with Eq.(3.20), we get the so-called Clausius-Mossotti relation

$$\alpha = \frac{\varepsilon - 1}{\varepsilon + 2}\frac{3\varepsilon_0 V}{N}, \tag{3.23}$$

relating the atomic polarizabiliy to the dielectric constant [1, p. 165-166].

3.3.2 Approximated ionic vibration; driven oscillator with damping

?? The frequency dependent permittivity $\varepsilon(\omega)$ is usually called the dielectric function. For insulators, $\varepsilon(\omega)$ is complex and energy can be resonantly transferred to the solid for certain frequencies. $\varepsilon(\omega)$ implies a frequency dependence of the refractive index $N(\omega)$. Most of the frequency dependence can be explained by a simple idea combined with knowledge about the polarization mechanisms and how the different polarization mechanisms manages to keep up with the oscillating electric field. E.g. orientation polarization and ionic polarization does not manage to oscillate fast enough at higher frequencies, while the atomic polarization will, see Figure 3.2.

For a quntitative description of the frequencydependence of ε we can consider a simplified version of ionic vibration. Light can couple to optical phonons, e.g in ionic crystals where the phonons correspond to an out-of-phase virbation of the positive and negative ions in the unit cell. These vibrations can be approximated by independent harmonic oscillators driven by an electric field $E^{-i\omega t}$, with one such oscillator per unit cell of the crystal. Each oscillator have a resonant frequency of $\omega_o = (2\gamma/M)^{1/2}$, where γ is the force constant and M is the reduced mass of the two ions. The motion is damped by a term proportional to the velocity $\eta dx/dt$ and represents the excitation of other vibrations in the material, due to the large displacement. The resulting equation of motion is that of a driven harmonic oscillator with damping

$$\frac{d^2x}{dt^2} + \eta\frac{dx}{dt} + \omega_0^2 x = \frac{eE}{M}e^{-i\omega t}. \tag{3.24}$$

A good ansatz for the solution is

$$x(t) = Ae^{-i\omega t}, \tag{3.25}$$

resulting in the amplitude

$$A = \frac{eE}{M}\frac{1}{\omega_0^2 - \omega^2 - i\eta\omega} \tag{3.26}$$

$$= \frac{eE}{M}\left[\frac{\omega_0^2 - \omega^2}{(\omega_0^2 - \omega^2)^2 + \eta^2\omega^2} + \frac{i\eta\omega}{(\omega_0^2 - \omega^2)^2 + \eta^2\omega^2}\right] \tag{3.27}$$

Using this as the ionic vibration, we can calculate the total polarization for a crystal with N unit cells and volume V. Considering only one type of ions with a density N/V and effective atomic polarizability α, assuming both ionic and atomic polarization, $P_i(\omega)$, $P_a(\omega)$, the result reads

$$P(\omega) = P_i(\omega) + P_a(\omega) = \frac{N}{V}eA(\omega)e^{-i\omega t} + \frac{N}{V}\alpha E e^{-i\omega t}. \tag{3.28}$$

When dealing with two types of ions like in a NaCl crystal, the different polarizabilities can be taken care of by a suitable definition of α. The resulting dielectric function can be calculated from

$$\varepsilon_0\varepsilon(\omega)E(\omega) = P(\omega) + \varepsilon_0 E(\omega), \tag{3.29}$$

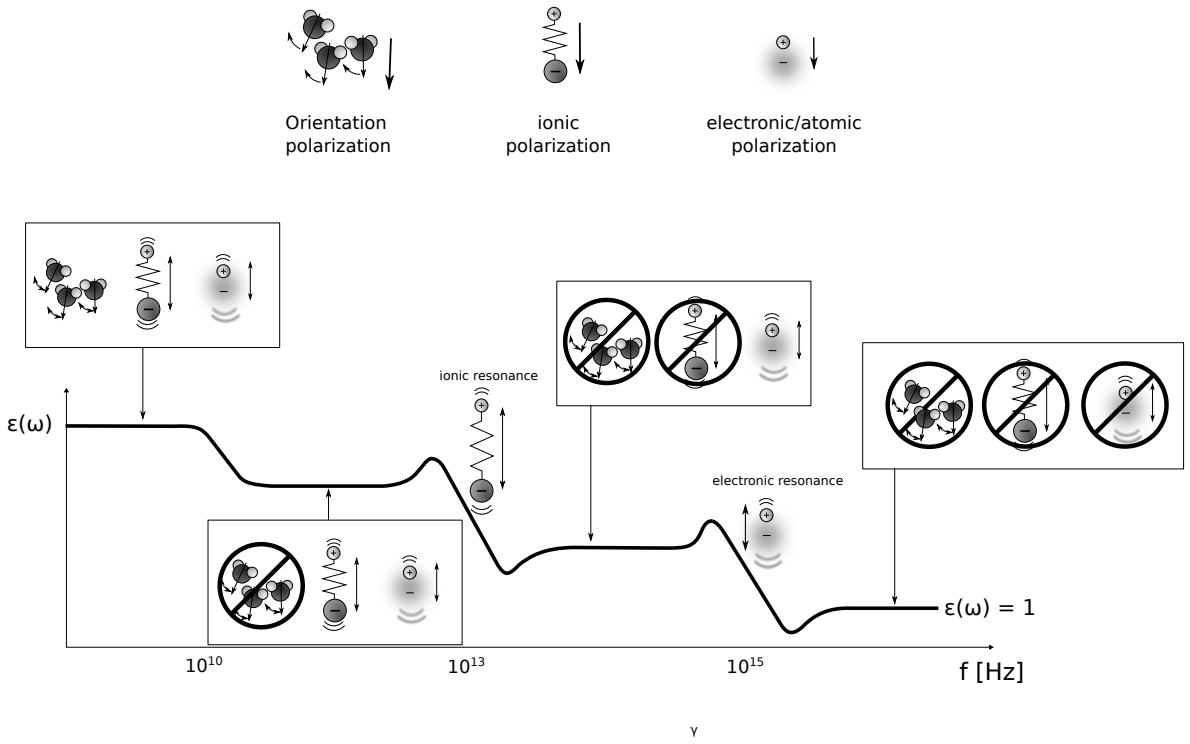

Figure 3.2: The contribution of orientation, ionic and electronic polarization. As the frequency of the applied electric field increases, the different polarization mechanisms fail to remain in step with the field when above a characteristic frequency. At sufficiently high frequencies the material no longer manages to polarize and the dielectric constant drops to 1, corresponding to the permittivity of free space. Note that in the discussion only the ionic and electronic contribution have been considered. The Figure is adapted from [3].

giving

$$\varepsilon(\omega) = \frac{P(\omega)}{\varepsilon_0 E e^{-i\omega t}} + 1 \tag{3.30}$$

$$= \frac{NeA(\omega)}{V\varepsilon_0} + \frac{N\alpha}{V\varepsilon_0} + 1 \tag{3.31}$$

$$= \frac{NeA(\omega)}{V\varepsilon_0} + \varepsilon_{opt}. \tag{3.32}$$

Here, ε_{opt} is the high frequency or optical limit, where the fields move to quickly for the ions to respond and $P_i(\omega) = 0$, i.e.

$$\varepsilon_{opt} = \lim_{\omega\to\infty} \varepsilon(\omega) = \frac{N\alpha}{V\varepsilon_0} + 1. \tag{3.33}$$

Plugging in the expression for $A(\omega)$ the real and complex values of the dielectric function $\varepsilon(\omega) = \varepsilon_{\Re e}(\omega) + i\varepsilon_{\Im m}(\omega)$ may be written as

$$\varepsilon_{\Re e}(\omega) = \frac{Ne^2}{V\varepsilon_0 M} \frac{\omega_0^2 - \omega^2}{(\omega_0^2 - \omega^2)^2 + \eta^2\omega^2} + \varepsilon_{opt}, \qquad \varepsilon_{\Im m}(\omega) = \frac{Ne^2}{V\varepsilon_0 M} \frac{\eta\omega}{(\omega_0^2 - \omega^2)^2 + \eta^2\omega^2} \tag{3.34}$$

The behaviour of the result is shown in Figure 3.3 The real part $\varepsilon_{\Re e}(\omega)$ is almost constant away from the resonance

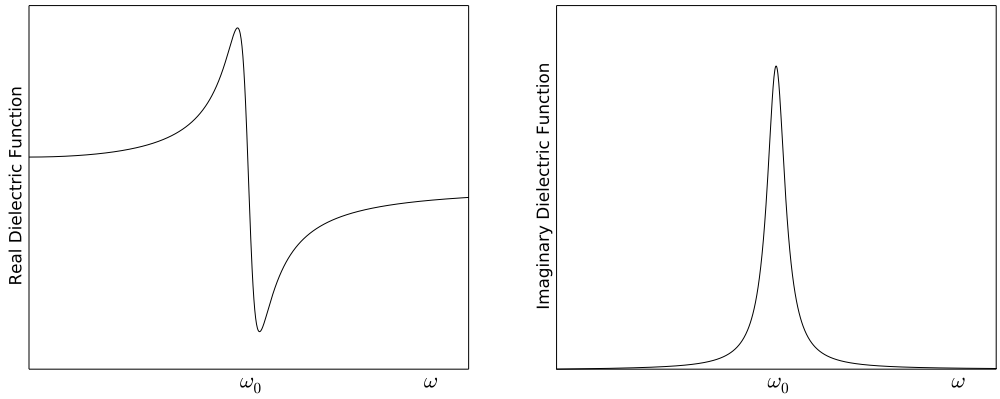

Figure 3.3: The dielectric function of a ionic crystal approximated by a driven harmonic oscillator with damping. The left and right figures show the behavior of the real and imaginary dielectric function close to the resonance frequency ω_0.

frequency, but its value is higher at lower frequencies due to the loss of the contribution from the ionic polarization. The imaginary part $\varepsilon_{\Im m}(\omega)$ is however zero everywhere except at the vicinity of the resonant frequency, where it shows a peak with a width given by the damping coefficient η.

To understand the meaning of $\varepsilon_{\Im m}(\omega)$ and that the width if its resonance peak is connected to the damping coefficient η, one can consider the energy dissipation in the system. The instantaneous electrical power dissipated per unit volume is given by

$$P(t) = j(t)E(t) = j(t)Ee^{-i\omega t} \tag{3.35}$$

where j(t) is the curent density. In an insulator, there are no free currents, only polarization currents

$$j(t) = -\frac{\partial D}{\partial t} = -\frac{\partial}{\partial t}\varepsilon\varepsilon_0 Ee^{-i\omega t} = i\omega\varepsilon\varepsilon_0 Ee^{-i\omega t} \tag{3.36}$$

The average dissipated power is found by averaging over one cycle $T = 2\pi/\omega$

$$P = \frac{1}{T}\int_0^T E(t)j(t). \tag{3.37}$$

If ε is purely imaginary, $j(t)$ is out of phase with $E(t)$ and their product will always give a nonzero negative value, $-\varepsilon_0\varepsilon_{\Im m}(\omega)E^2$. On the other hand, if ε is purely real, the phase shift will be $\pi/2$ and the integral will give $P = 0$. $\varepsilon_{\Im m}(\omega)$ is therefore a measure of the energy dissipation of the electric field due to the solid, and is obviously highest at the resonance.

The discussion explains some of the optical behaviour of the material. This is however not the entire picture. E.g. the frequency dependence in the visible and UV region is not explained here. These effects are due to the valence electrons, which would need a quantum mechanical description of the electronic structure of the solid. From the band structure of solids, a qualitative undestanding is obtainable. Figure 3.4 shows regions of high photon absorbtion due to the excitation of electrons, and how this affects the imaginary dielectric function $\varepsilon_{\Im m}(\omega) = \varepsilon_i(\omega)$. Note that the photons do not have enough energy to change the electrons wave vector [1, p. 166-171].

3.4 The electric potential, Laplace's equation and the Uniqueness Theorem

Before the following section, it might be beneficial to quickly recapitulate the basic relations for the electric potential from electrostatics. Instead of calculating the electric field directly from a given charge distribution, it is

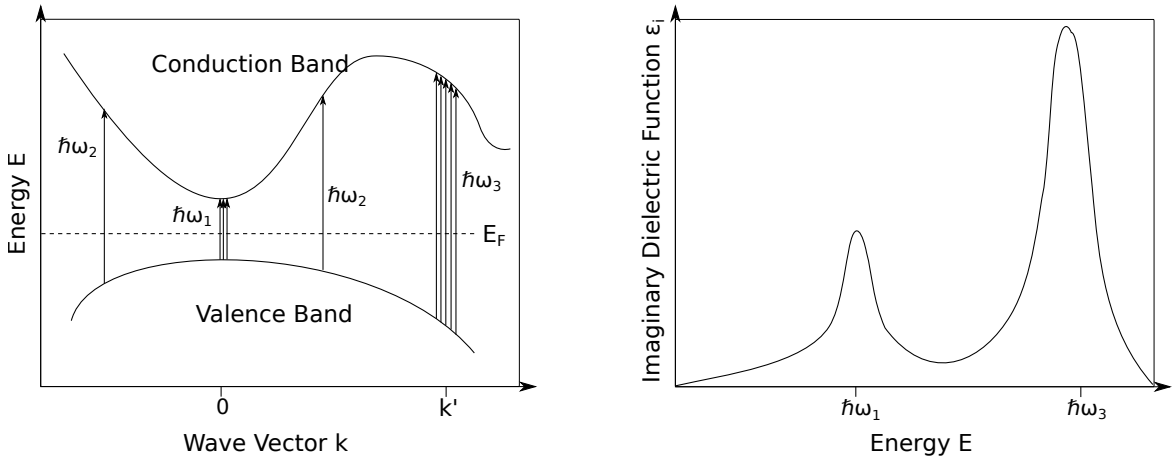

Figure 3.4: The left figure shows the photon-induced transitions between occupied and unoccupied states in the band structure of a solid. E_F is the fermi energy. In the regions where the valence band and conduction bads are parallel, a certain photon energy can excite several states. Here, the parallel regions are located at $\boldsymbol{k} = 0$ and $\boldsymbol{k} = \boldsymbol{k}'$ and result in higher transitions density. These transitions correspond to absorbtion of the electromagnetic wave given by the imaginary part of the dielectric function ε_i. The resulting resonances in ε_i due to the absorbtion of the $\hbar\omega_1$ and $\hbar\omega_2$ transitions are depicted in the right figure. The figure is adapted from [1, p. 170]

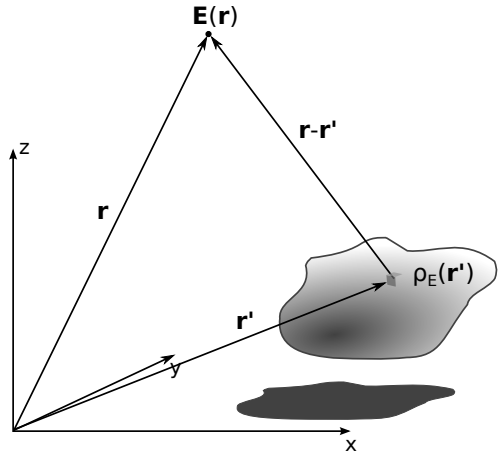

Figure 3.5: The electric field $\boldsymbol{E}(\boldsymbol{r})$ (at position $\boldsymbol{r}$) due to the charge distribution ρ_E located at $\boldsymbol{r}'$.

usually simpler to calculate the electric potential

$$\Psi(\boldsymbol{r}) = \frac{1}{4\pi\varepsilon_0}\int \frac{1}{|\boldsymbol{r}-\boldsymbol{r}'|}\rho(\boldsymbol{r}')d\boldsymbol{r}' \tag{3.38}$$

first and then calculate the electric field from

$$\boldsymbol{E} = -\nabla\Psi. \tag{3.39}$$

Here, ε_0 is the permittivity of vacuum and the other symbols can be understood from Figure 3.5. Often, this might also be too tough to handle analytically. In these situations it is better to solve Poisson's equation

$$\nabla^2 \Psi = -\frac{1}{\varepsilon_o}\rho, \tag{3.40}$$

which together with appropriate boundary conditions, is equivalent to Eq.(3.38). Very often, we are interested in finding the potential containing no charge, because the charge is located on the outside of our region of interest. In such cases Eq. (3.40) reduces to Laplace's equation [2, p. 110-111]

$$\nabla^2 \Psi = 0. \tag{3.41}$$

According to the *Uniqueness Theorems*, the solution to Laplace's equation is uniquely determined in some volume if the potential is specified on the boundary of the volume. This easily extends to Poisson's equation by further requiring that the charge distribution throughout the region is known.

The uniqueness theorem grants an enlarged mathematical freedom in the approach of finding the potential of a region of space. This is because the boundary uniquely determines the potential in the enclosed region and any approach giving the correct boundary conditions would give you the correct potential function through Laplace's equation Eq. (3.41). This allows the use of tricks, like for example the classical *method of images* [2, p. 116-121].

References

[1] Hofmann P. Solid State Physics, An Introduction. Wiley-VCH 2008; p.71-74,76-81

[2] Jensen B. The quantum extension of the Drude-Zener theory in polar Semiconductors. Handbook of optical constants of Solids, Five-Volume 1997 (1985??)(9)<-it's chapter 9;169-170

[3] . Dissemination of IT for the promotion of Materials Science (2000) Variation of the dielectric constant in alternating fields. University of Cambridge 2004: http://www.doitpoms.ac.uk/tlplib/dielectrics/variation.php (24. August 2015).

4 The theory behind GranFilm

This section discusses the theoretical background behind GranFilm, a software used to calculate the optical properties of granular thin films. The software implemented by Simonsen and Lazzari is based on the theory developed by Bedeaux and Vlieger [3] which introduces so called excess fields to handle the complexity of the surface. Before we dive into the details of this approach it might be beneficial to first consider scattering from flat surfaces.

4.1 Theoretical Introduction; Flat Surface Scattering

Starting from basic electromagnetic theory, the simplest case of electromagnetic scattering is the transmission and reflection of light, hitting a flat, smooth interface between two different half-infinite media. The electric permittivity ε and magnetic permeability μ of the media are given with subscript + for the upper media, and − for the lower media, see Figure 4.1. Assuming that the incoming electromagnetic wave is a plane wave, the reflection and transmission of the wave can be calculated from Maxwell's equations,

$$\nabla \cdot \boldsymbol{D} = \rho_f \qquad \nabla \times \boldsymbol{E} = -\frac{\partial \boldsymbol{B}}{\partial t} \tag{4.1a}$$

$$\nabla \cdot \boldsymbol{B} = 0 \qquad \nabla \times \boldsymbol{H} = \boldsymbol{J}_f + \frac{\partial \boldsymbol{D}}{\partial t}, \tag{4.1b}$$

which describe the general behavior of electromagnetic waves. Here the electric field $\boldsymbol{E}$, the electric displacement $\boldsymbol{D}$, the magnetic field $\boldsymbol{H}$ and the magnetic induction $\boldsymbol{B}$ are pairwise related through

$$\boldsymbol{D} = \varepsilon \boldsymbol{E}, \qquad \boldsymbol{H} = \frac{1}{\mu}\boldsymbol{B}, \tag{4.2}$$

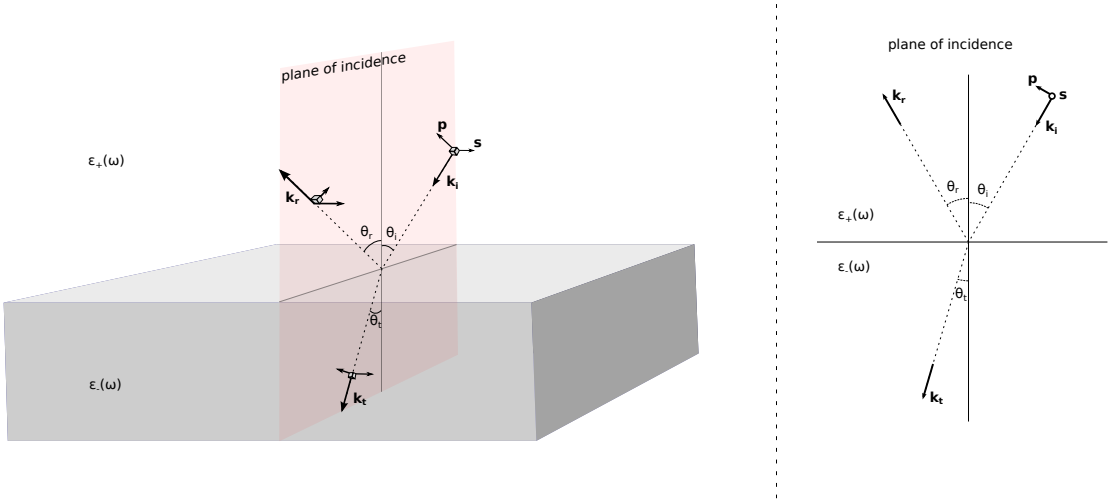

Figure 4.1: The reflection and transmission of an incident electromagnetic plane wave on a flat interface between two media. The dielectric functions for the upper and lower media are $\varepsilon_+(\omega)$ and $\varepsilon_-(\omega)$, respectively. The polarization direction $\boldsymbol{p}$ is the polarization parallel to or inside the place of incidence, while $\boldsymbol{s}$, which comes from the german word senkrecht meaning perpendicular, is the perpendicular polarization. The figure is adopted from ([1], p.125).

assuming linear media [2, p. 330]. Further assuming that there is no free charge or free current at the interface, Maxwell's equation provide the boundary conditions ([2], p.333)

$$D_\perp^+ = D_\perp^- \qquad \boldsymbol{E}_\parallel^+ = \boldsymbol{E}_\parallel^- \tag{4.3a}$$

$$B_\perp^+ = B_\perp^- \qquad \boldsymbol{H}_\parallel^+ = \boldsymbol{H}_\parallel^-. \tag{4.3b}$$

($\perp$ and $\parallel$ denotes the perpendicular and parallel komponent with respect to the surface boundary. By enforcing these boundary conditions on the incident, reflected and transmitted waves, on the entire boundary, the reflection and transmission coefficients may be calculated. The coefficients are given by

$$R \equiv \frac{I_r}{I_i} \qquad T \equiv \frac{I_t}{I_i}, \tag{4.4}$$

(4.5)

where $I_x, x \in [i, r, t]$ is the intensity or power per unit area stricking/leaving the interface for the incident, reflected and transmitted light, respectively [2, p. 386-391]. The calculation can be found in any standard optics textbook [2] and gives

$$R = r^2 \qquad T = \frac{n_- \cos\theta_t}{n_+ \cos\theta_i} t^2. \tag{4.6}$$

(4.7)

n_+ and n_- are the indices of refraction for the media above (+) and belov (-) the interface, while θ_i and θ_t gives the incident and transmitted lights direction with respect to the surface normal. The coefficients r and t are called the Frensel coefficients and their values depend on the polarization of the incident light. For the flat interface the coefficients take the form

$$r_s = \frac{n_+ \cos\theta_i - n_- \cos\theta_t}{n_+ \cos\theta_i + n_- \cos\theta_t} \qquad t_s = \frac{2n_+ \cos\theta_i}{n_+ \cos\theta_i + n_- \cos\theta_t}, \tag{4.8a}$$

$$r_p = \frac{n_- \cos\theta_i - n_+ \cos\theta_t}{n_+ \cos\theta_t + n_- \cos\theta_i} \qquad t_p = \frac{2n_+ \cos\theta_i}{n_+ \cos\theta_t + n_- \cos\theta_i} \tag{4.8b}$$

so the reflection and transmission are different for the two polarization directions [2, p. 121-123]. The two polarizations are illustrated in Figure 4.1

4.2 Scattering on rough surfaces: excess fields and surface susceptibilities

When moving away from a flat surface towards a more complicated geometry of the boundary between the two media, the corresponding dielectric function also becomes complicated. Situations like these might be encountered for rough surfaces or granular thin films, where the latter means that a foreign material is distributed as small island on top of a substrate. With such a complicated boundary, the calculation of the Fresnel coefficients becomes more difficult. [1, p. 125].

However, Bedeaux and Vlieger [3] developed an approach in which the exact knowledge of the electromagnetic fields close to the surface is not required. Their formalism is based on the notion of excess quantities. The excess fields are defined as the differene between the real fields and the bulk fields extrapolated to the surface, where the bulk field simply means the field given sufficiently far away from the scattering surface. E.g. for the electric field $\boldsymbol{E}(r)$ the excess quantity is defined as

$$\boldsymbol{E}_{ex}(\boldsymbol{r}) = \boldsymbol{E}(\boldsymbol{r}) - \boldsymbol{E}^{-}(\boldsymbol{r})\theta(-z) - \boldsymbol{E}^{+}(\boldsymbol{r})\theta(z), \tag{4.9}$$

where $\theta(z)$ is the Heaviside function and the superscript $\pm$ are used to indicate the region above (+) and below (-) the dividing interface at $z = 0$. In addition, the optical frequency ω is implicitly included in the notation. Furthermore, the excess field is only significant close to the surface, since $\boldsymbol{E}(\boldsymbol{r},\omega) \to \boldsymbol{E}^{\pm}(\boldsymbol{r},\omega)$ when $z \to \pm\infty$.
By integrating these excess fields along the z-axis, which is set normal to the surface,

$$\boldsymbol{D}^{s}_{\parallel}(\boldsymbol{r}) = \int_{-\infty}^{+\infty} dz\, \boldsymbol{D}_{ex,\parallel}(\boldsymbol{r}), \qquad E^{s}_{z}(\boldsymbol{r}) = \int_{-\infty}^{+\infty} dz\, E_{ex,z}(\boldsymbol{r}) \tag{4.10a}$$

$$\boldsymbol{B}^{s}_{\parallel}(\boldsymbol{r}) = \int_{-\infty}^{+\infty} dz\, \boldsymbol{B}_{ex,\parallel}(\boldsymbol{r}), \qquad H^{s}_{z}(\boldsymbol{r}) = \int_{-\infty}^{+\infty} dz\, H_{ex,z}(\boldsymbol{r}), \tag{4.10b}$$

and gathering them in a singular Dircac term, $\delta(z)$, located at the surface (z=0) (see Figure 4.2, the fields may be rewritten on the form (here shown for just the electric field)

$$\boldsymbol{E}(\boldsymbol{r}) = \boldsymbol{E}^{-}(\boldsymbol{r})\theta(-z) + \boldsymbol{E}^{s}(\boldsymbol{r})\delta(z) + \boldsymbol{E}^{+}(\boldsymbol{r})\theta(z). \tag{4.11}$$

Demanding that the fields given by Eq. (4.11) fulfill the Maxwell equations one ends up with the following boundary conditions

$$\left[\boldsymbol{E}^{+}_{\parallel}(\boldsymbol{r}) - \boldsymbol{E}^{-}_{\parallel}(\boldsymbol{r})\right]\Big|_{z=0} = i\omega\hat{z}\times\boldsymbol{M}^{s}_{\parallel}(\boldsymbol{r}_{\parallel}) - \nabla_{\parallel}P^{s}_{z}(\boldsymbol{r}_{\parallel}) \tag{4.12a}$$

$$\left[D^{+}_{z}(\boldsymbol{r}) - D^{-}_{z}(\boldsymbol{r})\right]\Big|_{z=0} = -\nabla_{\parallel}\boldsymbol{P}^{s}_{\parallel}(\boldsymbol{r}_{\parallel}) \tag{4.12b}$$

$$\left[\boldsymbol{H}^{+}_{\parallel}(\boldsymbol{r}) - \boldsymbol{H}^{-}_{\parallel}(\boldsymbol{r})\right]\Big|_{z=0} = i\omega\hat{z}\times\boldsymbol{P}^{s}_{\parallel}(\boldsymbol{r}_{\parallel}) - \nabla_{\parallel}M^{s}_{z}(\boldsymbol{r}_{\parallel}) \tag{4.12c}$$

$$\left[B^{+}_{z}(\boldsymbol{r}) - B^{-}_{z}(\boldsymbol{r})\right]\Big|_{z=0} = -\nabla_{\parallel}\boldsymbol{M}^{s}_{\parallel}(\boldsymbol{r}_{\parallel}), \tag{4.12d}$$

which is derived by Vlieger and Bedaux [3, p.21]. Here $\nabla_{\parallel}$ is the nabla operator parallel to the surface, while z denotes the vector component in the direction normal to the surface at $z = 0$. In addition, the quantities with superscript s are the so-called excess polarization and magnetization densities

$$\boldsymbol{P}^{s}(\boldsymbol{r}_{\parallel}) = \left(\boldsymbol{D}^{s}_{\parallel}(\boldsymbol{r}_{\parallel}),\ -\varepsilon_0 E^{s}_{z}(\boldsymbol{r}_{\parallel})\right) \tag{4.13a}$$

$$\boldsymbol{M}^{s}(\boldsymbol{r}_{\parallel}) = \left(\boldsymbol{B}^{s}_{\parallel}(\boldsymbol{r}_{\parallel}),\ -\mu_0 H^{s}_{z}(\boldsymbol{r}_{\parallel})\right), \tag{4.13b}$$

Here, in Eq.(4.13), the quantities on the right hand side are the integrated excess fields. Even though Maxwell's equations have been included, demanding that the fields follow the boundary conditions of Eqs.(4.12), they do not uniquely determine the physical situation. Maxwell's equations in matter, Eq.(4.1) given in Section 4.1, includes $\boldsymbol{E}$ and $\boldsymbol{D}$, together with $\boldsymbol{B}$ and $\boldsymbol{H}$, but does not state how they depend on eachother. In other words, Eq.(4.1) does not contain more information than Maxwell's equations given in free space. So, to fully explain how the fields interact with material and the interface, constitutive relations characteristic to the surface must be given (like the relations in Eq.(4.2) given for the flat interface example) [2, p. 330]. The constitutive relations link the

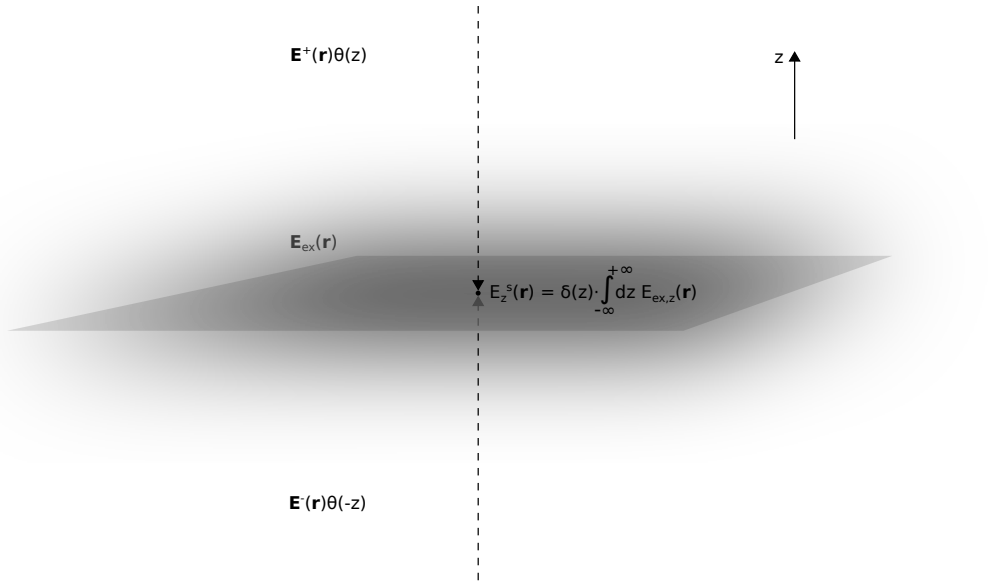

Figure 4.2: The excess fields are integrated over all values of z over the entire surface. Here this is vizualized for the eletric excess field, vizualized by the fog surrounding the surface, as the excess field, is only significant close to the surface. Note however that the excess field is complicated and not correctly represented by the fog. ([1], p.126).

interfacial polarisation and magnetization density $\left(\boldsymbol{P}^s(\boldsymbol{r}_\parallel)\right.$ and $\left.\boldsymbol{M}^s(\boldsymbol{r}_\parallel)\right)$ and the bulk fields extrapolated to the surface. If the pertubed surface layer thickness d is negligible compared to the optical wavelength λ, the excess fields are only significant or non-negligible close to the surface, which followed from the notation for the excess fields assumed earlier in Eq. (4.9). Because of this, the constitutive relations are local and the extrapolated bulk fields may be written on the form $\boldsymbol{E}_{\parallel,\Sigma} = \left\{\boldsymbol{E}^+_\parallel(\boldsymbol{r}_\parallel) + \boldsymbol{E}^-_\parallel(\boldsymbol{r}_\parallel)\right\}/2$. For simplisity we restrict our discussion to non-magnetic materials, i.e. that $\boldsymbol{M}^s(\boldsymbol{r}_\parallel) = 0$. The simplest constitutive relation can be written on the form

$$\boldsymbol{P}^s(\boldsymbol{r}_\parallel) = \xi^s_e\left[\boldsymbol{E}_{\parallel,\Sigma}(\boldsymbol{r}_\parallel),\ -D_{z,\Sigma}(\boldsymbol{r}_\parallel)\right]. \tag{4.14}$$

By further assuming that the interface is homogeneous and isotropic, the interfacial tensor reduces to a diagonal matrix [3, p. 30]:

$$\xi^s_e = \begin{bmatrix} \gamma & 0 & 0 \\ 0 & \gamma & 0 \\ 0 & 0 & \beta \end{bmatrix}, \tag{4.15}$$

With the first order surface susceptibilities γ and β. The reason why they are called first order susceptibilities is because the discussion above limits the dependence between the integrated excess quantities and the extrapolated bulk fields to a local relation (second order would require a spatial relation). In fact, even though they are not included in this discussion, GranFilm also takes account for the non-local dependence, described by the constitutive coefficients of second order δ and τ. These quantities are of the order d/λ smaller than the first order coefficients. Linear combinations of δ and τ together with the first order susceptibilities γ and β can construct invariants, which are independent of the choice of the separation surface. Furthermore, the Fresnel quantities, which all are measurable, are also independent of where we choose to put the surface in our coordinate system and can be uniquely expressed as a function of these constructed invariants. This discussion will continue to only consider the first order susceptibilities γ and β, which are the dominating factors when considering granular layers consisting of metallic islands [1]. **REFERANCE TO BEDEAUX AND VLIEGER????**

4.3 The Fresnel coefficients

Using the same method as for the flat Fresnel surface, the Fresnel coefficients in terms of the surface susceptibilities can be derived. The derivation is tedious and will not be done here. It can however be found in Bedeaux and Vlieger's book [3, p. 45]. The derivation follows the classical approach, but includes the excess field boundary conditions Egs.(4.12), together with the constitutive relations between the interface and the extrapolated bulk fields Eqs. (4.14). A property of this approach, is that the complicated surface approximated by the pertubed layer, does not change the fact of *Snell's law*, which pops out of the boundary conditions when calculating the classical flat surface problem Eq.[2, p. 388]. In other words,

$$\theta_i = \theta_r \tag{4.16a}$$

$$n_+ \sin\theta_i = n_- \sin\theta_t. \tag{4.16b}$$

is still used to find the angle of incidence θ_i, reflection θ_r and transmission θ_t. They are, so to speak, unmodified by the pertubed layer. However, the Fresnel coefficients, which decide the reflection and transmission amplitudes, do depend on the pertubed layer through the surface susceptibilities. For s-polarization, the resulting Fresnel coefficients are given by [1]

$$r_s(\omega) = \frac{n_- \cos\theta_i - n_+ \cos\theta_t + i(\omega/c)\gamma}{n_- \cos\theta_i + n_+ \cos\theta_t - i(\omega/c)\gamma} \tag{4.17a}$$

$$t_s(\omega) = \frac{2n_- \cos\theta_i}{n_- \cos\theta_i + n_+ \cos\theta_t - i(\omega/c)\gamma}. \tag{4.17b}$$

For p-polarization the expressions are a bit more complicated

$$r_p(\omega) = \frac{\kappa_-(\omega) - i(\omega/c)\gamma\cos\theta_i\cos\theta_t + i(\omega/c)n_-n_+\varepsilon_-\beta\sin^2\theta_i}{\kappa_+(\omega) - i(\omega/c)\gamma\cos\theta_i\cos\theta_t - i(\omega/c)n_-n_+\varepsilon_-\beta\sin^2\theta_i}, \tag{4.18a}$$

$$t_p(\omega) = \frac{2n_-\cos\theta_i\left[1 + (\omega/2c)^2\varepsilon_-\gamma\beta\sin^2\theta_i\right]}{\kappa_+(\omega) - i(\omega/c)\gamma\cos\theta_i\cos\theta_t - i(\omega/c)n_-n_+\varepsilon_-\beta\sin^2\theta_i}, \tag{4.18b}$$

where there has been introduced two quantites $\kappa_\pm$ defined as

$$\kappa_\pm = \left[n_+\cos\theta_i \pm n_-\cos\theta_t\right]\left[1 - \frac{\omega^2}{4c^2}\varepsilon_-\gamma\beta\sin^2\theta_i\right]. \tag{4.18c}$$

The simplicity of the expressions for s-polarization (4.17) compared to p-polarization (4.18), is due to the fact that s-polarized light only manages to excite modes parallel to the surface. This is reflected in the equations by the fact that $r_s(\omega)$ and $t_s(\omega)$ only depend on the parallel surface susceptibility γ. P-polarized light on the other hand, can excite modes both parallel and perpendicular to the interface, and gives rise to the increased complexity of $r_p(\omega)$ and $t_p(\omega)$, with the dependency of both γ and β.
If the surface susceptibilities in the expressions above are set to zero ($\gamma = \beta = 0$), this means that the perturbation from the flat interface, caused by the granular layer, disappears and the Fresnel coefficients, (4.17) and (4.18), reduce to the flat Fresnel coefficients, (4.8a) and (4.8b), respectively.

In addition to the source frequency ω, the refractive indices $n_\pm$ and the incident angle θ_i are input parameters. The three latter provide through Snell's law (4.16) the calculation of the angle of transmittance θ_t. However, the surface susceptibilies γ and β are not known and, in order to calculate the Fresnel coefficients for the pertubed surface layer, these quantities must be found.

4.4 Surface susceptibilities of island layer

To this point, there has been no assumptions regarding the geometrical nature of the surface layer. The kind of layer to be considered is a discontinuous thin film of nm-sized island, constituting a granular layer. If the islands are much smaller than the optical wavelength, the scattering from the granular film will be negligible and the resulting angular distribution of light will be similar to that of a flat interface ([**?**, p.11]. **<-???kan jeg bruke dette som referanse?sliter med å finne svaret i BV boka**. In this case, the density of islands, or the number of island per

unit surface area ρ, together with their ability to react to the applied field, , decide the surface polarization density $\boldsymbol{P}^s(\boldsymbol{r}_\parallel)$ [3, p. 99]

$$\gamma = \rho\alpha_\parallel \qquad\qquad \beta = \rho\alpha_\perp/\varepsilon_+^2 \tag{4.19}$$

The surface's ability to react to the applied field is called the polarizability α of the surface, where $\alpha_\parallel$ is the polarizability parallel to the surface, while $\alpha_\perp$ is perpendicular to the surface.

In other words, the optical properties in this situation is essentially driven by the polarizability of the island. The GranFilm software, supports the caulculation of both truncated spheres and truncated oblate or prolate spheroids. These two particle shapes can represent a great number of experimental situations, with the latter including shapes ranging from discs to needles [1, p. 128].

To calculate the surface polarizabilities, the first step is to solve Laplace's equation for the electrostatic potential

$$\nabla^2\Psi(\boldsymbol{r}) = 0 \tag{4.20}$$

in the quasi-static limit. An easy way to understand the quasistatic limit of Maxwell's equations is, as stated in [4, p. 238], to let $c \to \infty$, which would neglect all effects due to time retardation. This means that any charge or current distribution at any instant in time, would decide the resulting fields at the same instant, in all of space. In other words: the effect of the sources will be instantaneous. The validity of the result depends on the distance to the source and how fast the fields are fluctuating, making the approximation valid if the distances are sufficiently short or if the fluctuations of the fields are sufficiently slow [2, p.308-309]. In the case of the granular film, the approximation is valid for sub-wavelength-sized island, in correspondence to the assumption of the layer thickness compared to the wavelength of the incident light.
Assuming spherical island geometry, the potential can be expanded in a multipolar basis of seperable solutions to the electrostatic laplace equation, Eq.(4.20) [3, p. 78]

$$\Psi(\boldsymbol{r}) = \sum_{lm} A_{lm} r^{-l-1} Y_l^m(\theta,\phi) + \sum_{lm} B_{lm} r^l Y_l^m(\theta,\phi) \tag{4.21}$$

Here (r, θ, ϕ) are the spherical coordinates centered at the expansion point, A_{lm} and B_{lm} are the multipole expansion coefficients and $Y_l^m(\theta,\phi)$ are the spherical harmonics. The coordinate system for the expansion is given in Figure 4.3, with μ denoting the center of expansion, which may be centered at the truncated sphere or varied along the vertical symmetry axis. To deal with the boundary truncating the sphere, the classical image technique is used [1]. This is done by having a image expansion center located at the opposite side of the surface, compared to μ, inside the substrate. The image expansion point is denoted by $\bar{\mu}$. As shown in Figure 4.3, mathematical approach assumes 4 different media, even though region 4 is part of the substrate. When specifying the material in the software region 2 and 4, which constitute the substrate, are usually set to be the same. Using Eq.(4.21) to expand the potential around the expansion center and the image, the potential in the different regions take the form:

$$\Psi_1(\boldsymbol{r}) = \Psi_i(\boldsymbol{r}) + \sum_{lm}^{l\neq 0} A_{lm} r_\mu^{-l-1} Y_l^m(\theta_\mu,\phi_\mu) + \sum_{lm}^{l\neq 0} A_{lm}^r r_{\bar{\mu}}^{-l-1} Y_l^m(\theta_{\bar{\mu}},\phi_{\bar{\mu}}) \tag{4.22a}$$

$$\Psi_2(\boldsymbol{r}) = \Psi_t(\boldsymbol{r}) + \sum_{lm}^{l\neq 0} A_{lm}^t r_\mu^{-l-1} Y_l^m(\theta_\mu,\phi_\mu) \tag{4.22b}$$

$$\Psi_3(\boldsymbol{r}) = \psi_0(\boldsymbol{r}) + \sum_{lm}^{l\neq 0} B_{lm} r_\mu^l Y_l^m(\theta_\mu,\phi_\mu) + \sum_{lm}^{l\neq 0} B_{lm}^r r_{\bar{\mu}}^l Y_l^m(\theta_{\bar{\mu}},\phi_{\bar{\mu}}) \tag{4.22c}$$

$$\Psi_4(\boldsymbol{r}) = \psi_0(\boldsymbol{r}) + \sum_{lm}^{l\neq 0} B_{lm}^t r_\mu^l Y_l^m(\theta_\mu,\phi_\mu) \tag{4.22d}$$

Here, the $r^l\big|_{l=0}$ terms of the expansion are constant and have been extracted, giving the value $\psi_0(\boldsymbol{r})$ inside the sphere, corresponding to region 3 and 4 in Figure 4.3. The negative terms $r^{-1-l}\big|_{l=0} = r^{-1}$ represents free charge, wich has been assumed to be zero, and are removed [3, p. 79]. Outside the sphere, i.e. region 1 and 2, the potential is set to zero simply because the potential reference point can be chosen freely. In addition to the $l = 0$-terms, the incident field gives rise to the potential $\Psi_i(\boldsymbol{r})$. Some of the incident light is transmitted directly into the substrate

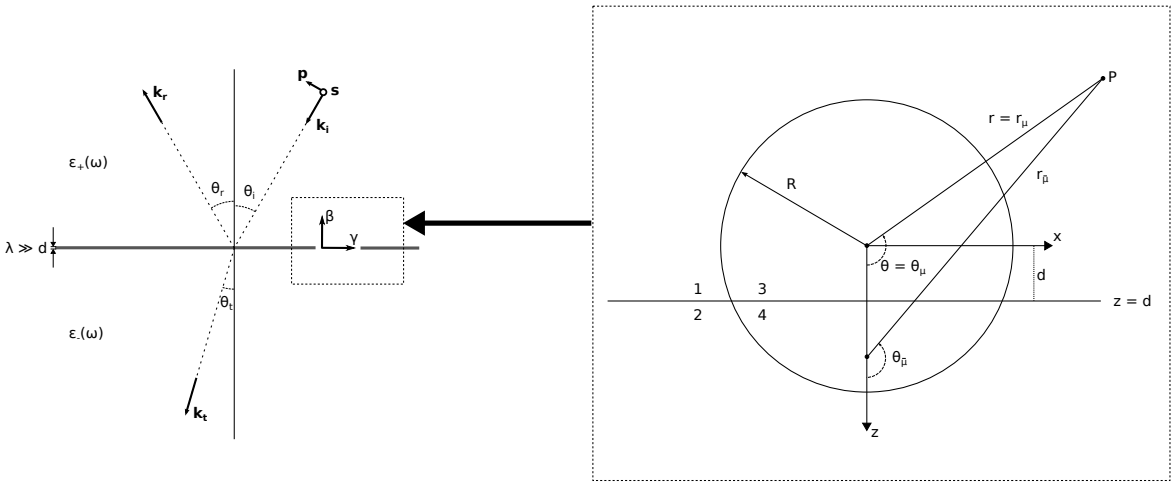

Figure 4.3: To the left: the transmission and reflection of a pertubed surface layer with thickness d, which is assumed to be much smaller than the optical wavelength λ of the incoming wave. The reflection and transmission amplitudes depend on the surface susceptibilities. The first order surface susceptibilities, γ and β, describe the ability of the surface to polarise in the parallel or perpendicular direction. These coefficients can be calculated from evaluating the geometry of the trunctated spheres (shown to the right), making up the granular thin film ([1], p.126). Adopted from ([1], p.125)

and the resulting scalar field is given by $\Psi_t(\boldsymbol{r})$. **Burde kanskje ta med at $\Psi_i(\boldsymbol{r})$, $\Psi_t(\boldsymbol{r}) \sim -\boldsymbol{r}\cdot\boldsymbol{E}_0$. Ref fra: [3, p. 95]** Comparing Eqs. (4.22) to Eq. (4.21), it is worth to note that all the r^l-terms in region 1 and 2, r^{-l-1}-terms in region 3 and 4 are removed due to the divergence of the potential as $r \to \infty$ and $r \to 0$, respectively.

The boundary conditions for the electric potential is given by [2, p. 89-90]

$$\varepsilon_i(\omega)\ \partial_n\Psi_i(\boldsymbol{r}) = \varepsilon_j(\omega)\ \partial_n\Psi_j(\boldsymbol{r}) \qquad\qquad \Psi_i(\boldsymbol{r}) = \Psi_j(\boldsymbol{r}) \tag{4.23}$$

where $\partial_n = \hat{n}\cdot\nabla$ is the derivative with respect to the normal direction $\hat{n}$ to the boundary surface, and the indicies $i, j \in \{1,2,3,4\}$, $i \neq j$ denotes the different media included at the different boundaries. From the boundary conditions, handled by the method of images [2, p. 121], the relation between the multipole coefficients are found

$$A^r_{lm} = (-1)^{l+m}\frac{\varepsilon_1-\varepsilon_2}{\varepsilon_1+\varepsilon_2}A_{lm} \tag{4.24a}$$

$$A^t_{lm} = \frac{2\varepsilon_1}{\varepsilon_1+\varepsilon_2}A_{lm} \tag{4.24b}$$

$$B^r_{lm} = (-1)^{l+m}\frac{\varepsilon_3-\varepsilon_4}{\varepsilon_3+\varepsilon_4}B_{lm} \tag{4.24c}$$

$$B^t_{lm} = \frac{2\varepsilon_3}{\varepsilon_3+\varepsilon_4}B_{lm}. \tag{4.24d}$$

However, there are still 4 unknowns for each multipole order, i.e. for every configuration of l and m. By using the orthogonality of the spherical harmonics $Y^m_l(\theta,\phi)$ to treat the boundary of the sphere, called the weak formulation of the boundary conditions, give two infinite linear systems for the multipolar coefficients A_{lm} and B_{lm} for $l = 1$, $m = 0, \pm 1$. To solve this system in practive, some cut-off value $l = M$ for the expansion is set. Based on investigations by Simonsen and Lazzari [5] a truncation at $M = 16$ appeared to be sufficient in most cases. This result is based on post-checking the boundary condition for the potential and the normal displacement at the surface; and convergence tests of the first term of the multipolar expansion. Keep in mind, that for cases like spherical caps (truncated at the upper hemisphere) or entire spheres on top of a substrate the convergence could be slower,

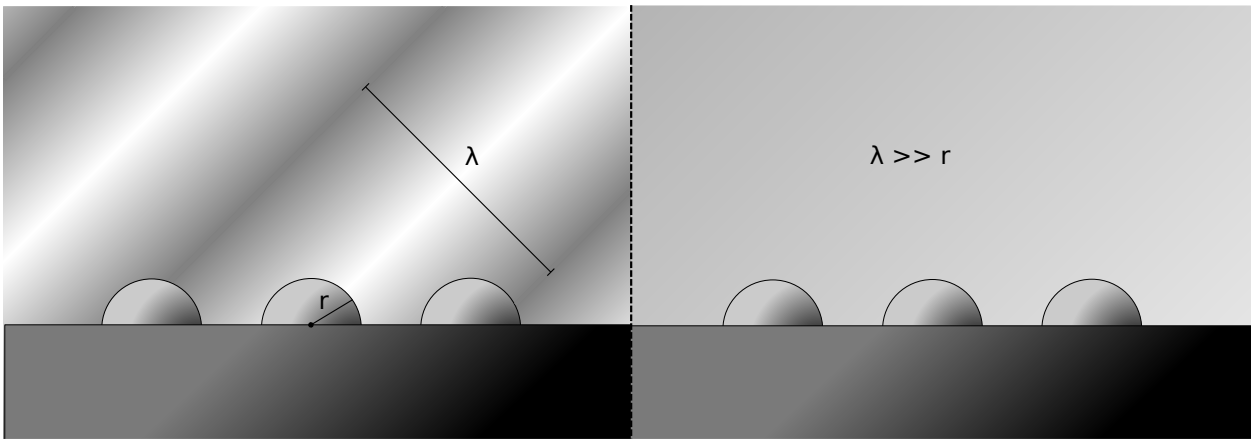

Figure 4.4: When the size and separation of the particles are small compared to the optical wavelength of the incident electromagnetic wave the particles are approximately excited by the same field. Here the greyscale of the background represent the amplitude of the field.

requiring a truncation $M > 16$. Finally, knowing the first multipolar coefficients the polarizability of the islands can be found

$$\alpha_\perp \simeq A_{10} \qquad\qquad \alpha_\parallel \simeq A_{11}. \tag{4.25}$$

The first $l = 0$ terms of region 1 A_{lm} are representing the dipole contribution, which dominates in the far-field limit [3, p. 99]

4.5 Inter-island coupling; collective contribution

So far, the discussion has only included the response of a single island and would perhaps give resonable result in the low coverage limit. However, this would lead to an increase in error for larger covarages and create the need for a correction due to the increasing island-island interaction for higher coverages [**?**, p. 20]. **<- Can I use this??????????????.**By assuming that the island are sufficiently close to one another such that their mutual separation is negligible compared to the optical wavelength, a correction to the low-coverage result can be obtained. In this limit, the islands would be excited by the same incident field and have similar responses to the field. See Figure 4.4. Assuming a dipole response, the islands would be affected by the dipole fields excited in the neighboring particles. If the spheres are truncated by the substrate through their lower hemisphere, the modified polarizabilities compared to the isolated polarizatilities, $\alpha_\perp, \alpha_\parallel$, become [3, p. 181]

$$\alpha_\perp^{\text{mod}} = \frac{\alpha_\perp}{1 - 2\alpha_\perp I_\perp^{20}} \qquad\qquad \alpha_\parallel^{\text{mod}} = \frac{\alpha_\parallel}{1 + 2\alpha_\parallel I_\parallel^{20}}. \tag{4.26}$$

The defined functions in the correction are called the interaction functions [1]

$$I_\perp^{20} = \frac{1}{\sqrt{20\pi} L^3 \varepsilon_-} \left[S_{20} - \left(\frac{\varepsilon_- - \varepsilon_+}{\varepsilon_- + \varepsilon_+} \right) \tilde{S}_{20}^r \right] \tag{4.27a}$$

$$I_\parallel^{20} = \frac{1}{\sqrt{20\pi} L^3 \varepsilon_-} \left[S_{20} + \left(\frac{\varepsilon_- - \varepsilon_+}{\varepsilon_- + \varepsilon_+} \right) \tilde{S}_{20}^r \right], \tag{4.27b}$$

where

$$S_{20} = \sum_{i \neq 0} \left(\frac{L}{r} \right)^3 Y_2^0(\theta, \phi) \Big|_{r = R_i} \tag{4.28a}$$

$$S_{20}^r = \sum_{i \neq 0} \left(\frac{L}{r} \right)^3 Y_2^0(\theta, \phi) \Big|_{r = R_i^r} \tag{4.28b}$$

are the direct and image lattice sums, describing the interaction with the other direct and image dipoles, respectively. L stands for the lattice constant. The $i = 0$ term in the summation gives the contribution from the interaction with the corresponding image of an island. This is taken into account when calculating the isolated response and is therefore not needed in Eq.(4.28). The validity of the dipolar approximation was tested by Lazzari and Simonsen for hemispherical silver islands layed out in a hexagonal pattern on a MgO substrate [1, p. 129-130] The polarizabilities were computed for $M = 16$ and showed that the relative error of the dipole approximation compared quadrupole approximation is $sim1\%$ up to 40% coverage, which is higher than the interesting limits encountered in experiments.

REFERENCES

[1] Lazzari R, Simonsen I. GranFilm: a software for calculating thin-layer dielectric properties and Fresnel coefficients. Thin Solid Films 2002;419:124-136 *ER DETTE RIKTIG?*

[2] Griffiths DJ. Introduction to electrodynamics, third edition. Pearson, international edition 2008.

[3] Bedeaux D, Vlieger J. Optical properties of surfaces. Imperial College Press, second edition 2004.

[4] Larsson J. Electromagnetics from a quasistatic perspective. American Association of Physics Teachers, 2007. **??Er denne riktig???**

[5] Simonsen I, Lazzari R. Jupille J, Roux S. Numerical modeling of the optical response of supported metallic particles. Physical Review B, 61(11):7722-7733, 2000.

[6] Lie LA, Simonsen I. Optical properties of a thin film of coated, truncated spheres. NTNU 2010. Imperial College Press, second edition 2004. **?FJERN DENNE!**

5 METHOD

By searching through various scientific articles, thermochromic data for a material in the form of either a complex dielectric constant $\varepsilon(\omega, T)$ or complex refrective index $N(\omega, T)$ was found. By the use of a program called ENGAUGE DIGITIZER graphically represented data, such as graphs or plots, could be extracted for use in numerical calculations. ENGAUGE DIGITIZER is a open source digitizing software and can be found on http://digitizer.sourceforge.net/. It can convert image files of type `.bmp, .jpeg` or other, containing a graph or a map, into numbers. The conversion from graphical to numerical data is obtained through defining three points the image, e.g. the origin, largest x-value and largest y-value for a function y = f(x), which define the x,y-axes together with their scale. The target data can be marked automatically or manually, depending on the quality of the image. The data can then be exported to a spreadsheet and used in numerical calculation.

Of the extracted data, only the data from Kang et al. [1, p. 3] were used, for reasons being that these were the only data that overlapped with the relevant data from the material database for GRANFILM. Kang et al. provided data for the dielectric constant of VO_2 as functions of energy, with one graph per temperature. The data were then interpolated in order to provide $\varepsilon(E, T)$ for $E \in [0.5eV, 4.0eV]$, $T \in [25^\circ C, 80^\circ C]$. It would be interesting to include data from several thermochromic materials. However, the ease of the data extraction with ENGAUGE DIGITIZER dependens on the quality and degree of overlap of the functions and could be very tedious. Further extractions have therefore not been prioritized. **??Should I say this, or is it best to leave it out???**

The material data input to be read by GRANFILM must however be on a specific form. GRANFILM requires a complex refractive index N as a discrete function of energy or wavelength. The real and imaginary values of N must be given for each point of its domain. In addition, the values of the domain must consist of equdistant values. The resulting data through the use of ENGAUGE DIGITIZER is not equidistant and because the real and imaginary data is usually extracted from different image files, their values do not correspond to the same discrete domain.

Because of this mismatch between the extracted image data, using ENGAUGE DIGITIZER, and the input file format of GRANFILM, some conversion had to be done. The data was converted to the form $N(E, T) = n(E, T) + ik(E, T)$ as a function of equidistant energy steps, with $[E]$=eV, and could now be fed into GRANFILM.

5.1 CHOICE OF PARAMETERS

Due to the quasistatic approximation where it was assumed that the layer thickness or the size of the particles should be negligible compared to the wavelength of the incident light $R \ll \lambda$. Here R is the radius of the island. In addition, the separation of the particles should be so small that they are excited by the same incident field, i.e. the lattice constant $L \ll \lambda$. Since the simulation computes for optical wavelengths down to about about 350nm, the simulation was run for $r \in [10\text{nm}, 15\text{nm}]$ with $L = 45\text{nm}$.

5.2 SIMULATION

Because of the response of the granular layer in the visible region and due to the reports on the unattractive colors of VO_2 thin films [10], the color was investigated using the free software COLORPY. COLORPY is a Python package that convert physical descriptions of light, such as light intensities, into RGB colors. The resulting colors are only approximate due to both the model and the monitor used to display the colors [3]. But because the uncertainties of the extracted data using ENGAUGE DIGITIZER, the analysis is primarily qualitative and the resulting colors is assumed to be adequate. **?!?!?Er dette greit å skrive?!?!?!?!?**

REMEMBER TO COMMENT OUT THIS (choise of parameters):

- talk about the corresponding intervall we're simulating (the energy range and the corresponding wavelength range).
- Then talk about how large sphere sizes we're then allowed to use.
- relate this up towards the mentioned thicness mentioned by the sources and comment on it.
- (...)can not use the thin optimal film layer thickness between 40-90nm as mentioned by Kamalisarvestani et al. [1] and Blackman et al. [10].

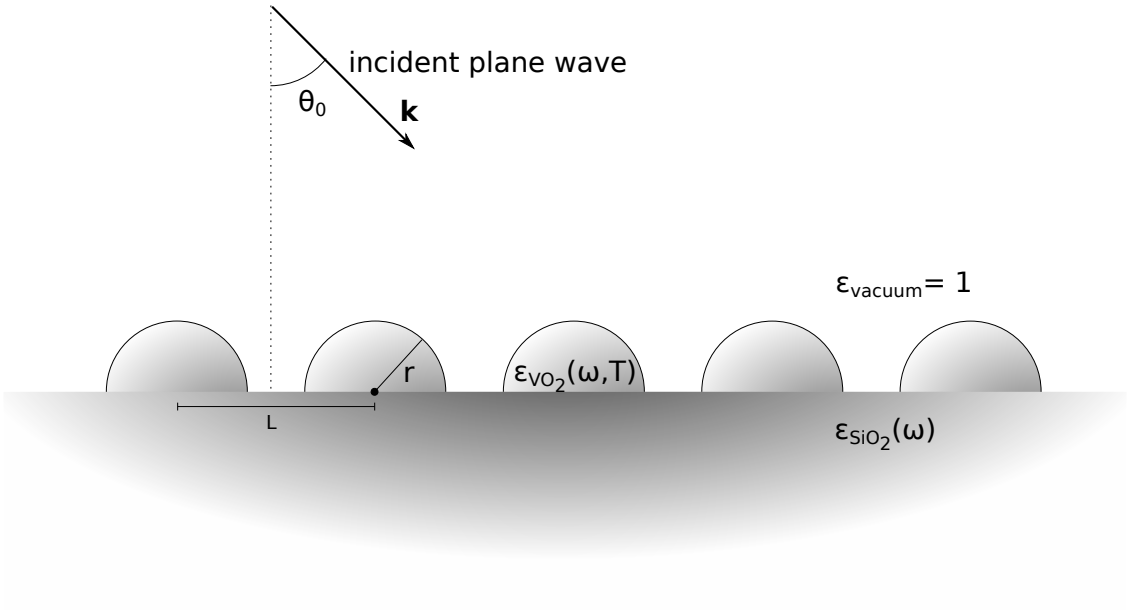

Figure 5.1: The simulation was run for a VO_2 particles supported by a SiO_2 substrate. The surrounding medium was set to vacuum with dielectric constant $\varepsilon = 1$. VO_2 is assumed to be the only material displaying temperature dependent behavior.

- the region of interest based on the introduction is the visible range (ϵ~[400,800nm] or [3-4eV,1eV]) and the IR range (ϵ~[800nm,10^5-10^6nm] or [1eV,10^{-3}eV]) [2, p. 11]

REFERENCES

[1] Kang M, Kim SW, Ryu JW, Noh T. Optical properties for the Mott transition in VO2. AIP Advances 2012;2,012168 **Er dette greit? Finner ikke sidetall osv.**

[2] Smith GF, King TA, Wilkins D. Optics and photonics: an introduction (second edition). Wiley 2007.

[3] . Kness M, ColorPy – A python package for handling physical descriptions of color and light spectra. 2008: http://markkness.net/colorpy/ColorPy.html (23. September 2015).

6 RESULTS

The following simulations were done with an incident plane wave of direction $(\theta_i, \phi_i) = (45°, 0°)$ on VO_2 particles supported by a SiO_2 substrate with truncation ratio $t_r = 0$. The surrounding medium is air with $\varepsilon = 1$, see Figure 5.1. The particles are arranged in a square lattice with lattice constant $L = 45$nm and the particle-particle interaction is given by a dipole contribution. The multipole truncation is set to $M = 16$. Figure 6.9 shows the surface

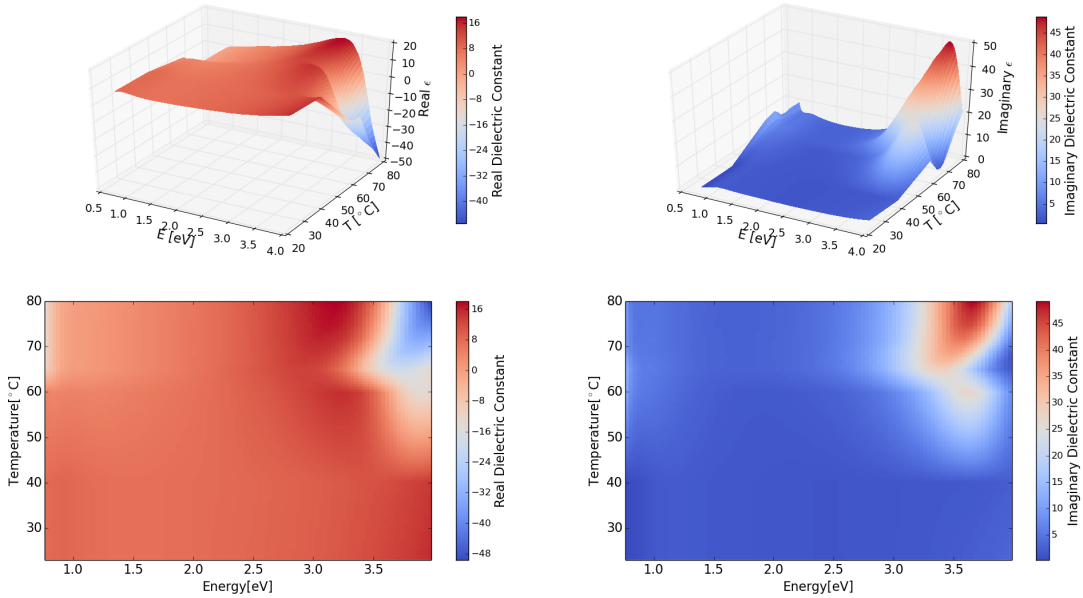

Figure 6.1: The interpolated dielectric function $\varepsilon(E,T)$ extracted from Kang et al. [1, p. 3].

differential reflectivity

$$\frac{\Delta R}{R} = \frac{R - R_0}{R_0} \tag{6.1}$$

where R is the total reflectivity and R_0 is the bare sufrace, or Fresnel, reflectivity [1].

There are two resonances, one in the IR or low energy region and one at higher energies, just above the visible region. The peak of the IR resonance is fairly stationary, shifting slightly to the right for increasing temperature, before shifting a bit back again. See Figure 6.3. Looking back at Figure 6.9, one can see a more dramatic change in the resonance located above the visible region. The top of the peak is first seen of about 45°C and shifts to higher energies with increasing amplitude to about 55-65°C. For higher temperatures the response decrease and, based on Figure 6.9a and 6.2b, it seems as the peak of the amplitude shifts back to lower energies.

Based Figure 6.9,6.3 and 6.4, one can see that the general behavior of the granular thermochromic layer is approximately the same, except for the amplitude. Because of these similarities, only the results for $r = 15$ will be explored further, as the reflective response is larger and therefore more interesting.

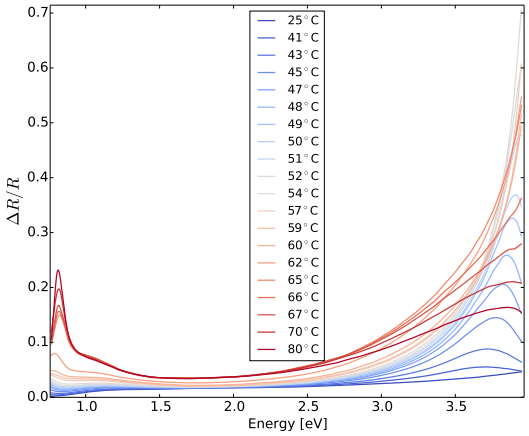

(a) $r = 10$, p-polarization.

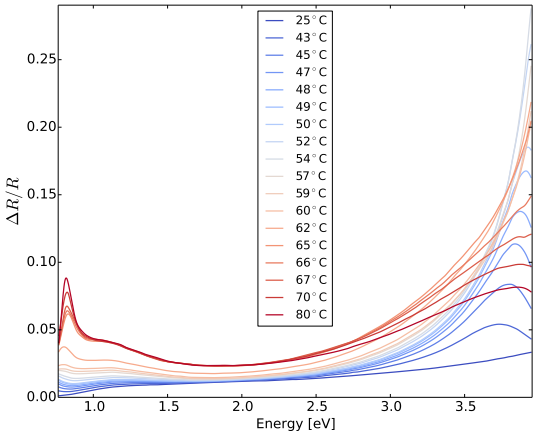

(b) $r = 10$, s-polarization.

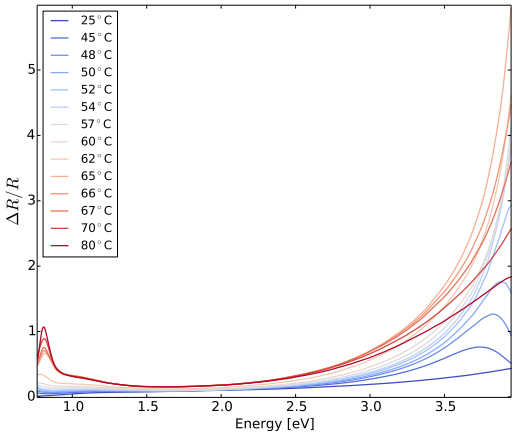

(c) $r = 15$, p-polarization.

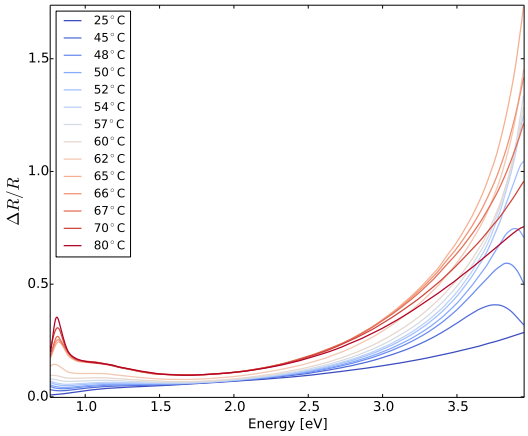

(d) $r = 15$, s-polarization.

Figure 6.2: Relative reflectance $\Delta R/R$ For different radii. The temperatures are chosen in order to show the behavior as the temperature increases.

6.1 Simulation 3; $R = 15$nm, p-polarized incident light

The surface polarizability and susceptibility is shown in Figure 6.6, 6.5. Both the parallel and perpendicular polarizability increases substantially for energies lower than 1.0 eV and higher than 2.5 eV. Between 1.0 to 2.0 eV, however, it experiences a decrease.

References

[1] Lazzari R, Simonsen I, Bedeaux D, Vlieger J, Jupille J. Polarizability of truncated spheroidal particles supported by a substrate: model and applications. The European Physical Journal B 2001; 24:267-284

6.2 Color

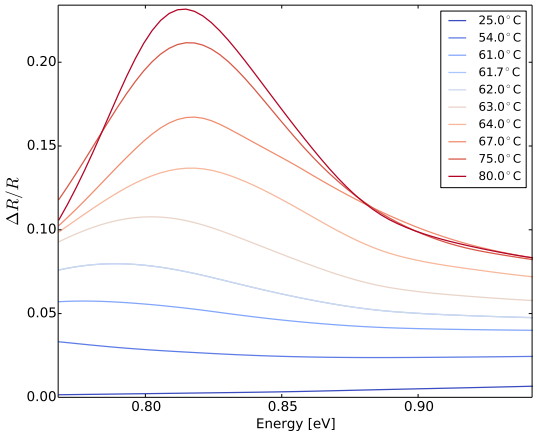

(a) $r = 10nm$, p-polarization

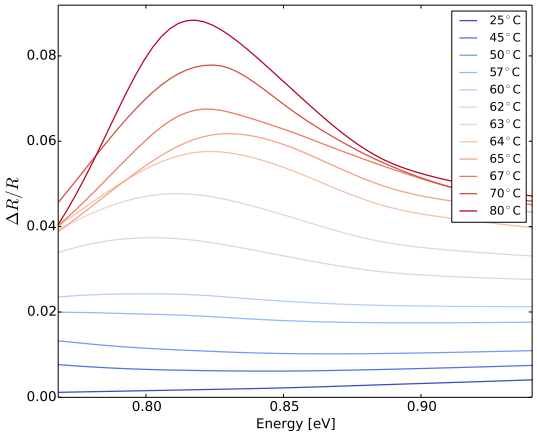

(b) $r = 10nm$, s-polarization

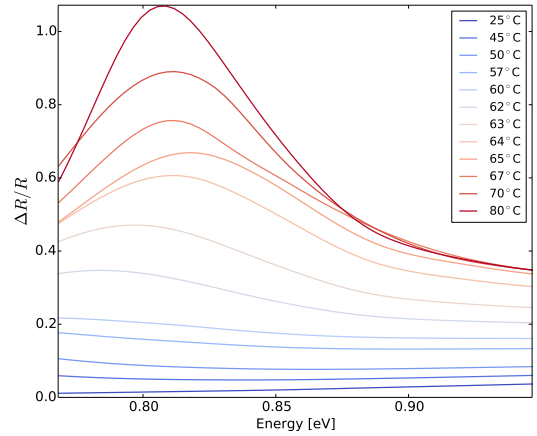

(c) $r = 15nm$, p-polarization

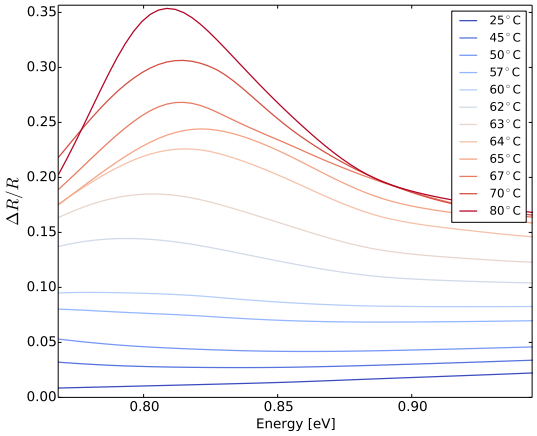

(d) $r = 15nm$, s-polarization

Figure 6.3: Relative reflectance in the IR region $\Delta R/R$.

7 DISCUSSION

Based on the litterature, the optical properties of vanadium dioxide should change drastically around the transition temperature 68°C, where it should change from a semi-conductor behavior, being less reflective, to a more reflective metallic state. In Section **??**, some of the reasons behind the frequency dependence of the dielectric function were discussed. Figure 6.1 shows increasing activity in the high energy region, at about 3.7eV, just above the visible range. There is also some activity in the low energy region below 1.0 eV, starting at around 60°C. This seems to fit with the resulting resonances seen in the differential reflectivity, shown in Figure 6.9. Furthermore, notice that the response for p-polarized is larger than for s-polarized light. This makes sense as p-polarized light can excite both parallel and perpencidular modes Eq.(4.18), while the response due to s-polarized light is only due to parallel modes Eq.(4.17).

As argued in the simplified discussion, it is expected that the modes should show some dependence on the surface polarizability. The surface polarizability and susceptibility in Figure 6.6, 6.5 shows a strikingly simiar behavior and only seem to differ in magnitude. One might be tempted to conclude a relation accoaring to Eq.(4.19), with $\varepsilon_+ = 1$. However, even though these simulations were carried out using the same island density ρ, Figure 6.7 shows that

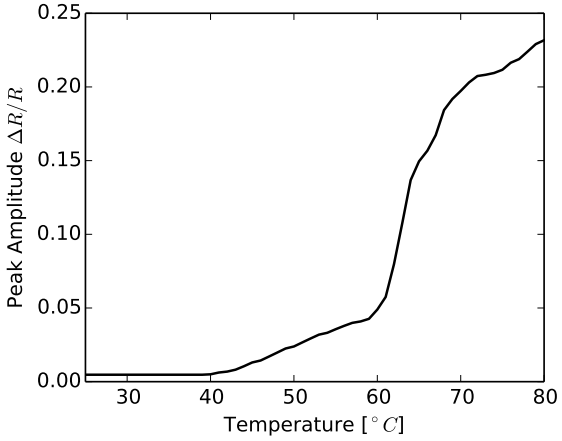

(a) $r = 10nm$, p-polarization

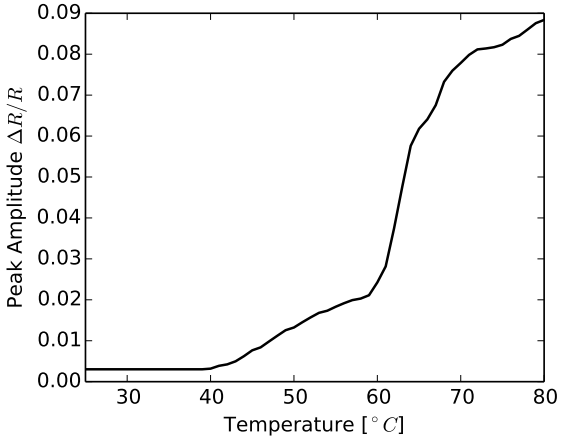

(b) $r = 10nm$, s-polarization

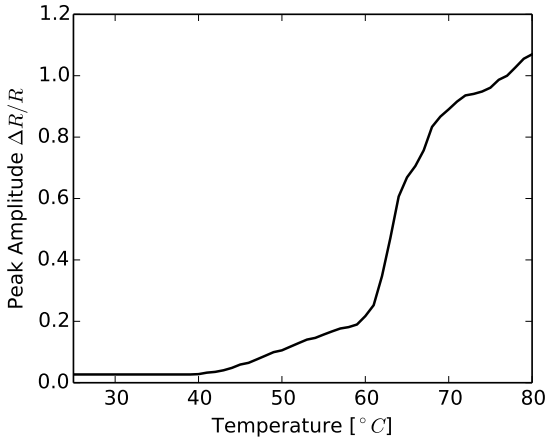

(c) $r = 15nm$, p-polarization

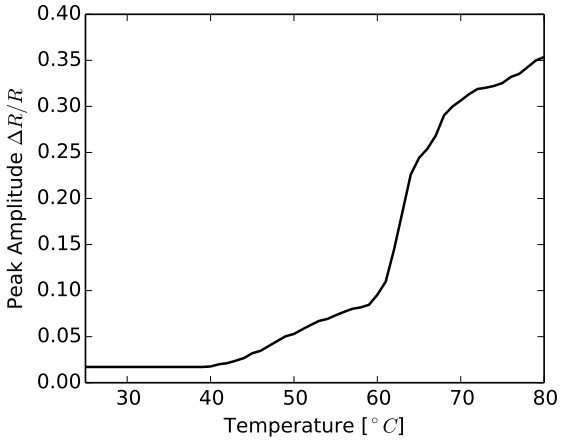

(d) $r = 15nm$, s-polarization

Figure 6.4: The IR resonance's peak amplitude of $\Delta R/R$, see Figure 6.3.

the relation is far more complicated than stated in the theoretical discussion. Still, for low temperatures the ratio seems to be approximately constant, at at least for $\alpha_\parallel$, and of the order ~ 0.1. Compared to the island density $\rho = 1/L^2 \approx 0.0005$ this is also an indication that there are some effects not covered in the simplified theoretical introduction. **???Should I say this? Can I say this???**

Looking at the peak in the IR region, Figure 6.3 and 6.4, the temperature dependence seem to follow the same behavior for both $r = 10$nm and $r = 15$nm, except that the latter has a larger peak amplitude of roughly a factor of 4.

- Check transmission for consistensy. Check if this seems valid/physical or else i have a problem.
- Discuss the resonance in the reflectance and compare it to the interpolated dielectric function. This will allow to include the theory of the frequency dependent dielectric function.
- Discuss the resonance in terms of the polarizabilities/surface susceptibilities. Compare the resonances.
- Talk about the behaviour of the reflectance. Does this make sense with what we already know about VO_2? Does this support VO_2 as a good smart window candidate?

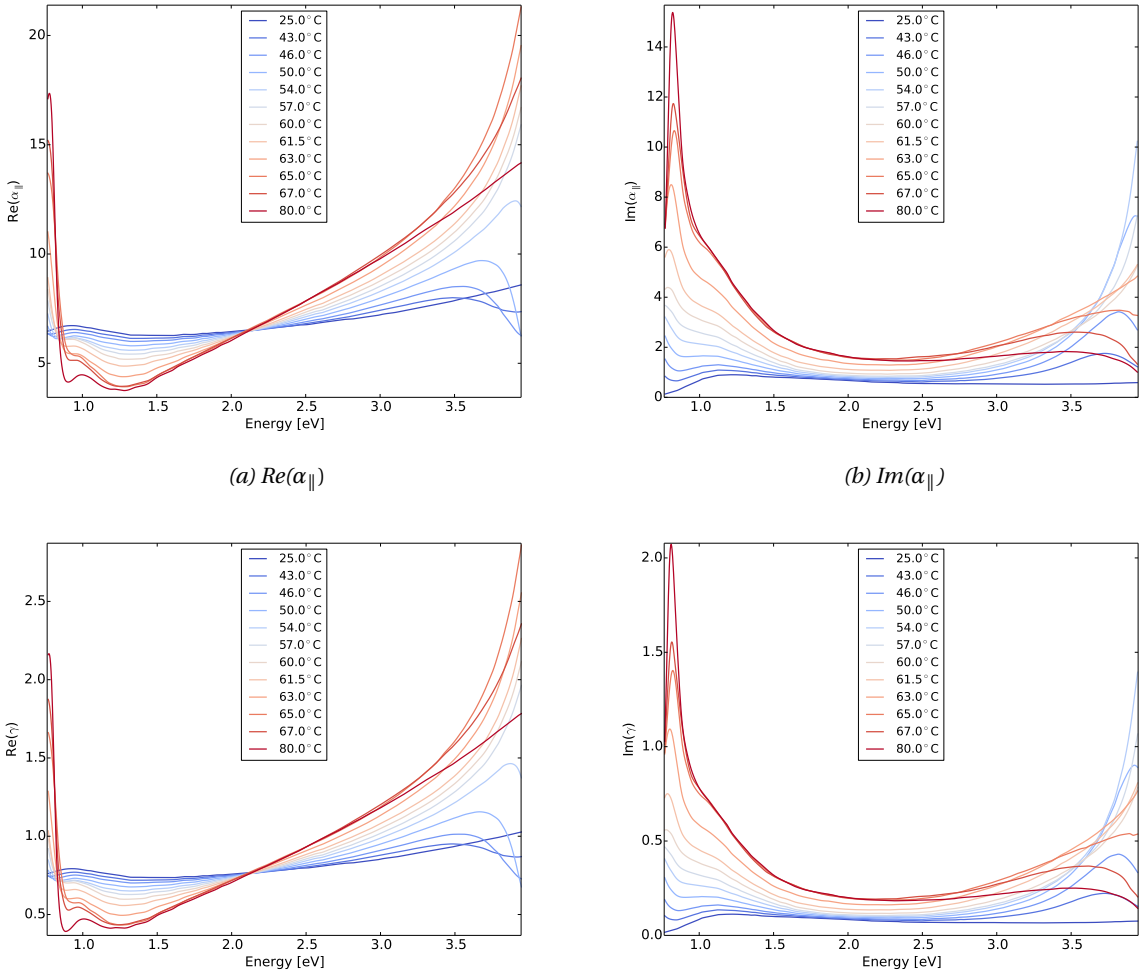

(a) Re($\alpha_{\parallel}$)

(b) Im($\alpha_{\parallel}$)

(c) Re(γ)

(d) Im(γ)

Figure 6.5: The perpendicular polarizability $\alpha_{\perp}$ and the surface susceptibility β.

- Also drag in the color, since this is also related to the smart window. Maybe also comment on (if i've mentioned it earlier) that I didn't get the yellow/green ish color. only blue. But, I've also only tried thicknesses of around 10-15nm radiuses.

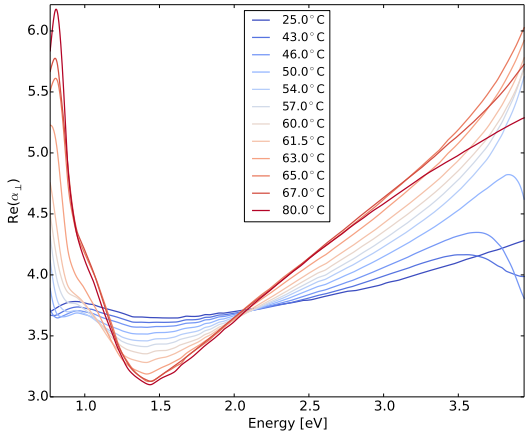

(a) Re($\alpha_\perp$)

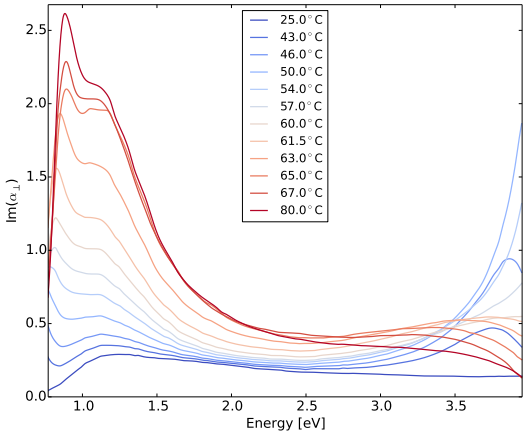

(b) Im($\alpha_\perp$)

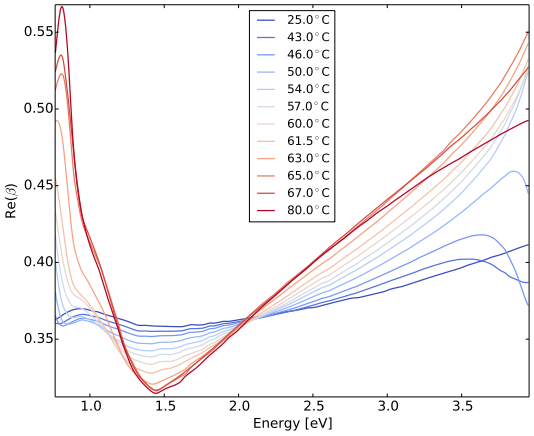

(c) Re(β)

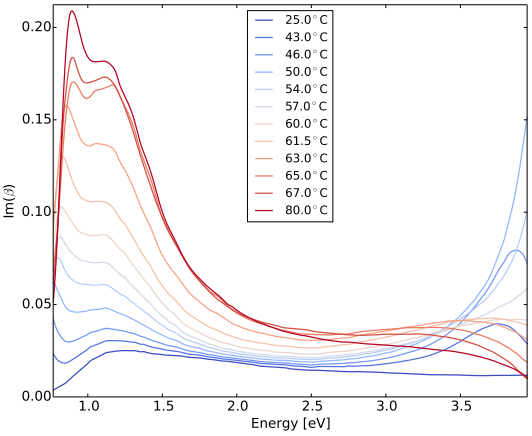

(d) Im(β)

Figure 6.6: The parallel polarizability $\alpha_\parallel$ and the surface susceptibility γ.

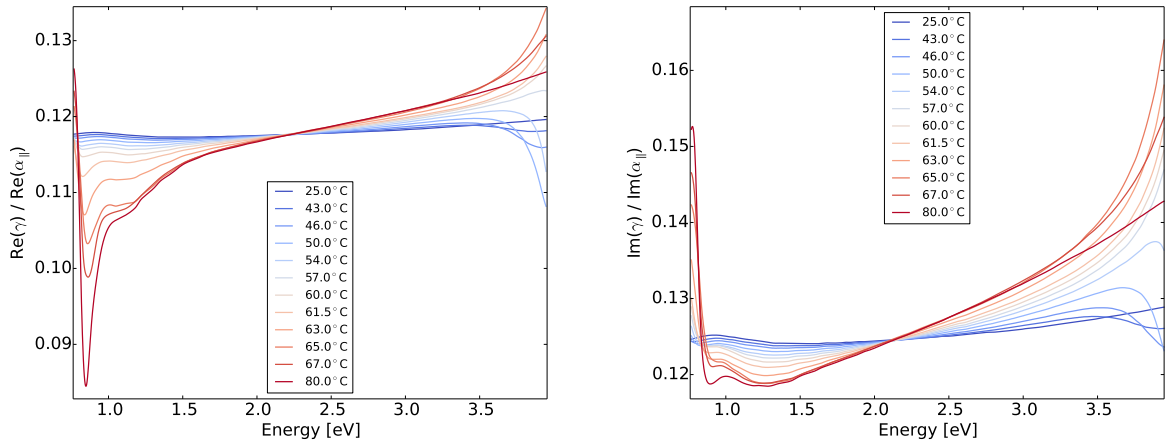

(a) re($\alpha_\perp$)

(b) im($\alpha_\perp$)

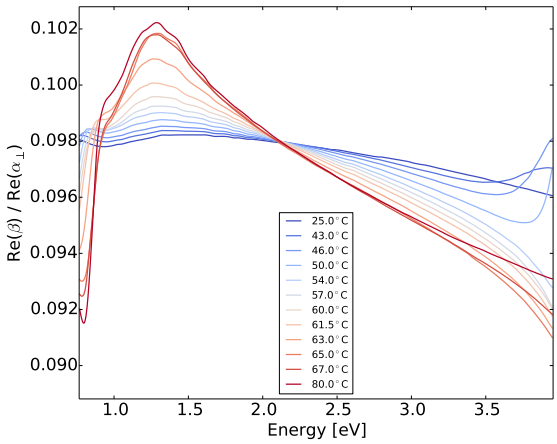

(c)

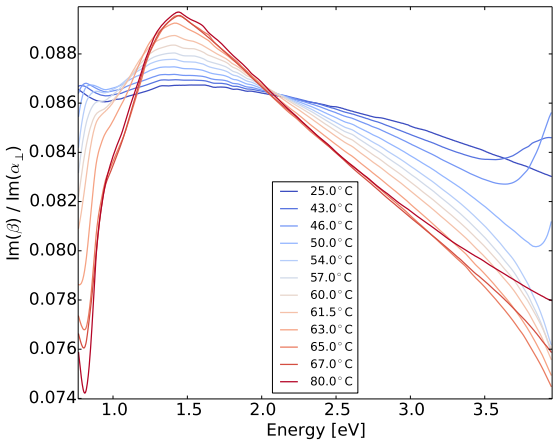

(d)

Figure 6.7: The ratio between the surface polarizabilities and the corresponding surface susceptibilities.

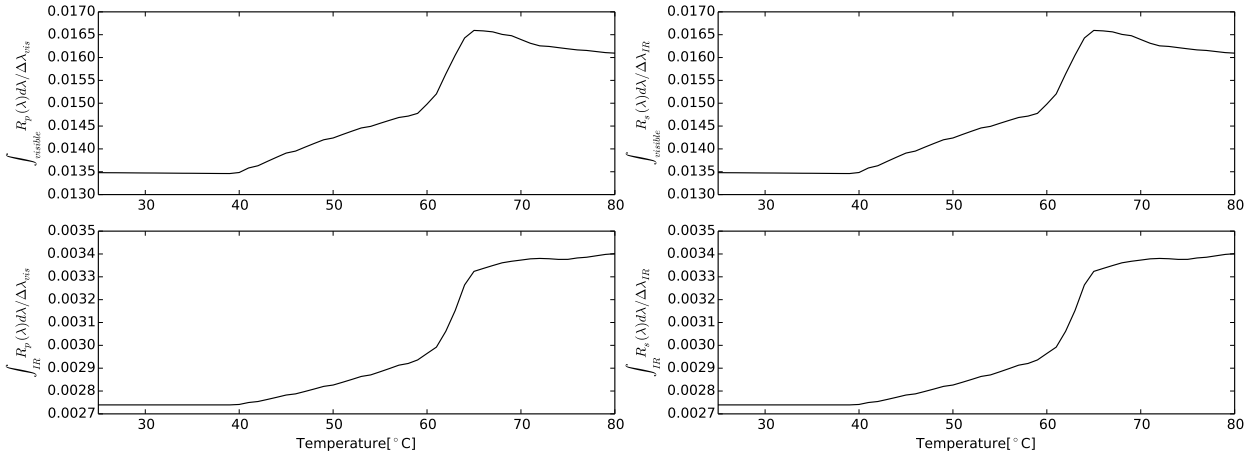

(a) $\theta_i = 45°$

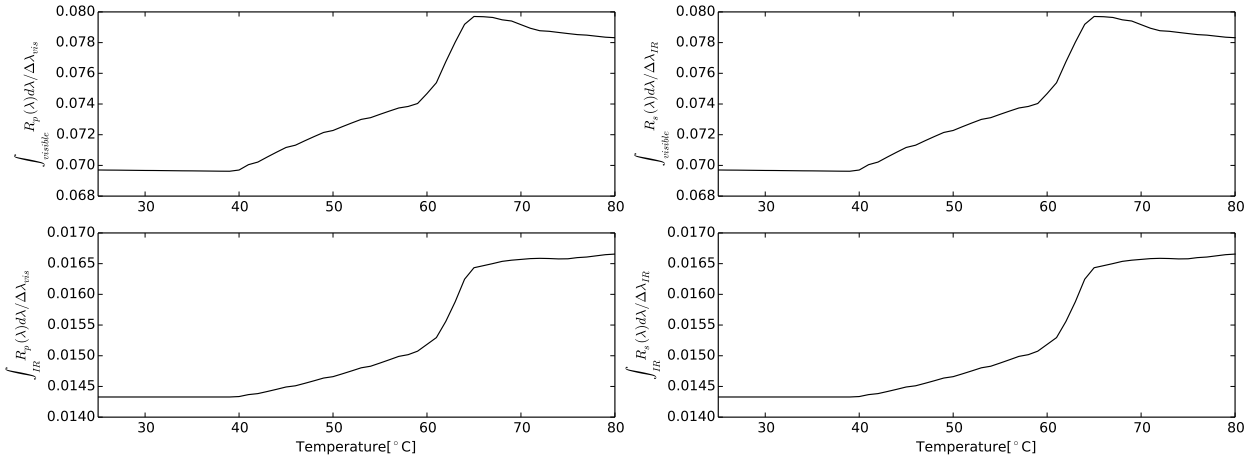

(b) $\theta = 0^\circ_i$

Figure 6.8: The integrated reflectance R for both p- and s-polarization. For each subfigure, simulated for different angle of incidence, the above figures show the integrated reflectance in the visible region 380-780nm, while the lower figures show for 780nm to about 1600nm in the near IR region.

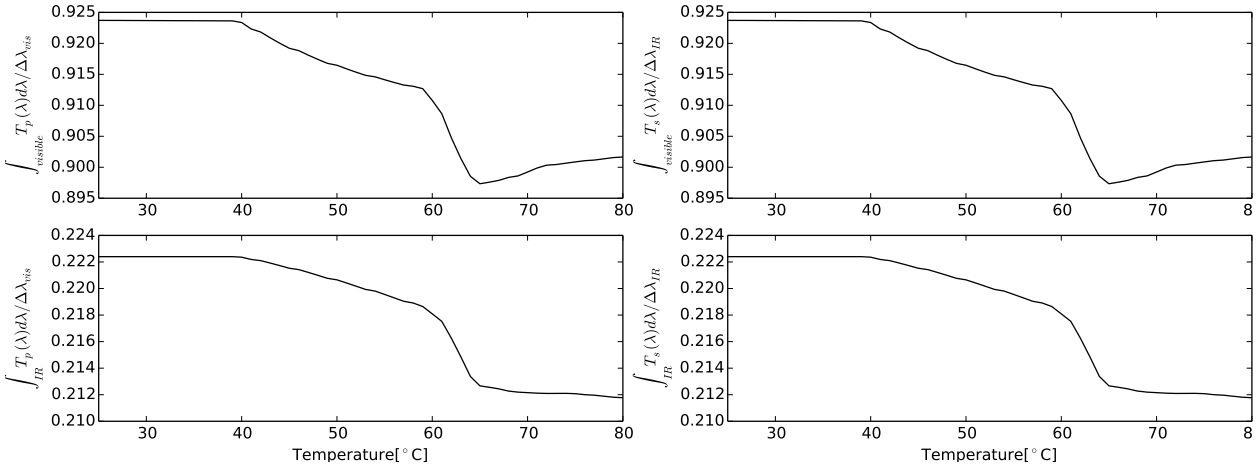

(a) $\theta_i = 45°$

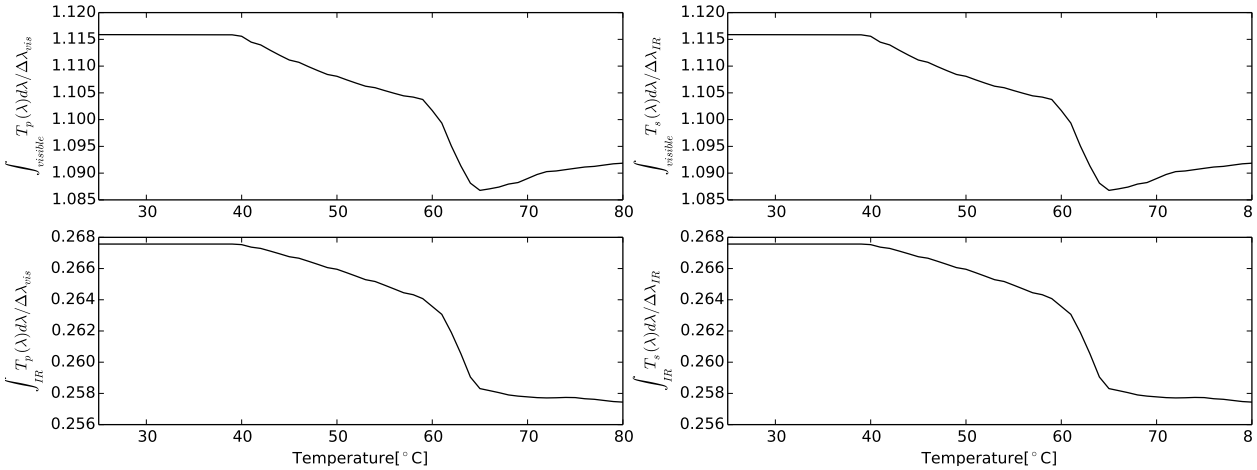

(b) $\theta = 0_i^\circ$

Figure 6.9: The integrated transmittance T for both p- and s-polarization. For each subfigure, simulated for different angle of incidence, the above figures show the integrated reflectance in the visible region 380-780nm, while the lower figures show for 780nm to about 1600nm in the near IR region.

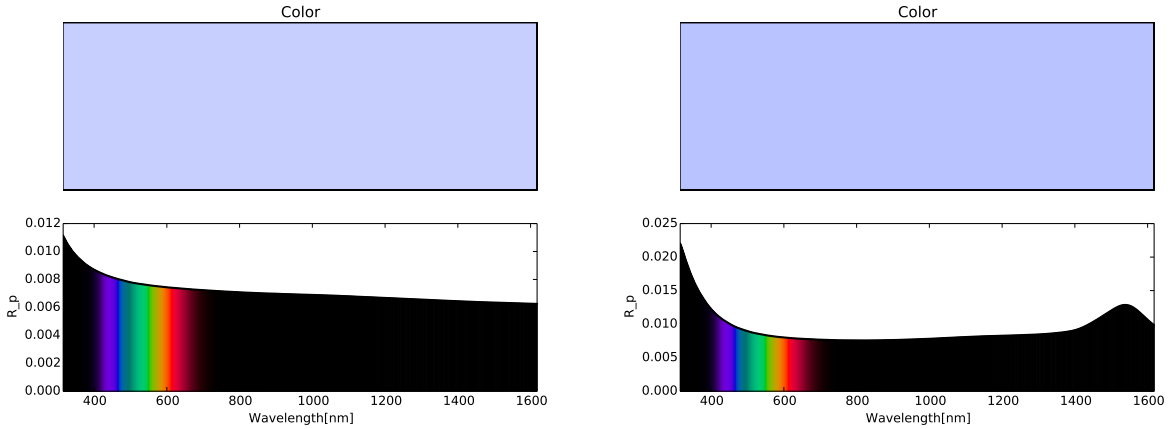

(a) $T = 25°C$ *(b)* $T = 80°C$

Figure 6.10: The spectral reflectance for p-polarization together with the approximate resulting color. The simulation was done $r = 15$.

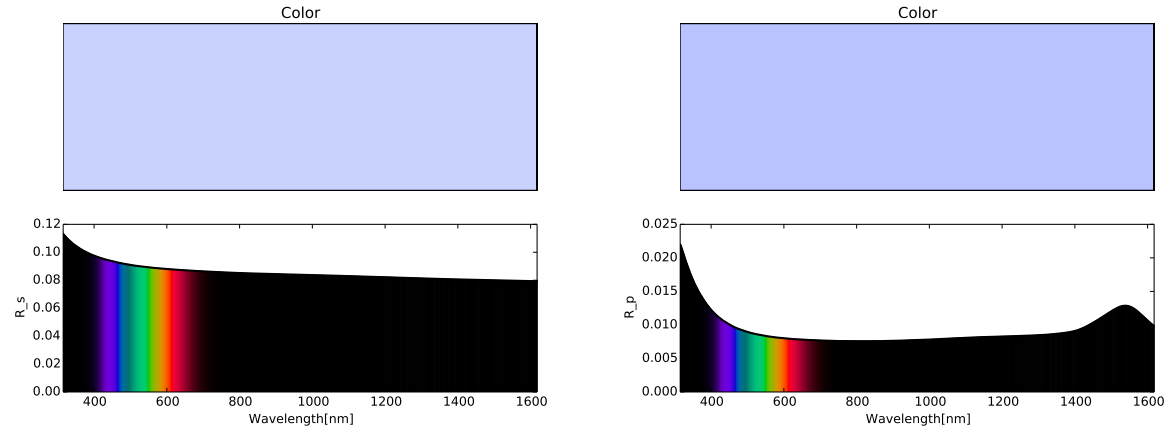

(a) $T = 25°C$ *(b)* $T = 80°C$

Figure 6.11: The spectral reflectance for s-polarization together with the approximate resulting color. The simulation was done $r = 15$.

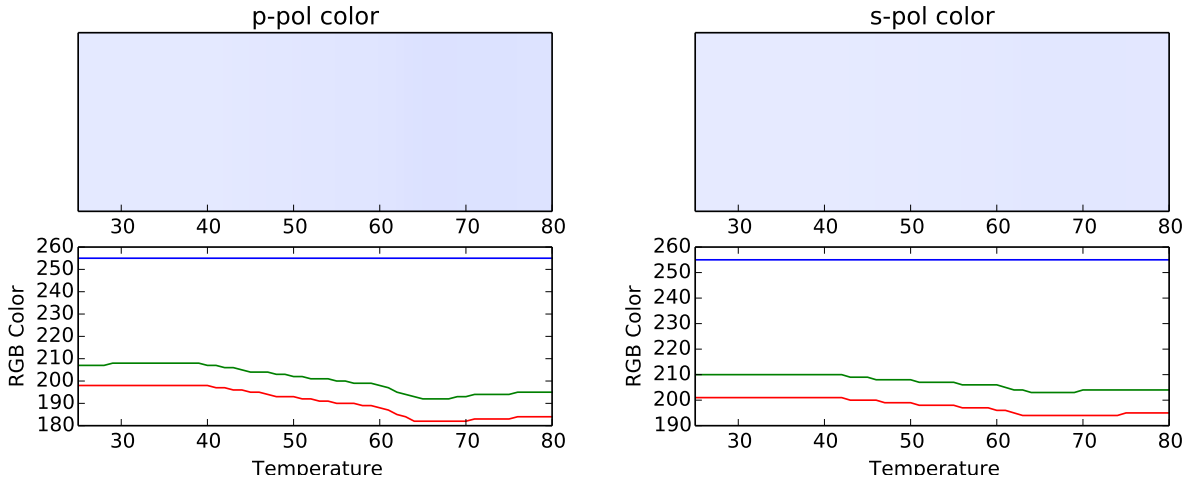

(a) p-polarization

(b) s-polarization

Figure 6.12: The resulting approximated color together with the corresponding RGB values, based on the reflectance with $r = 15$ *as a function of temperature.*